Article

From naproxen repurposing to naproxen analogues and their antiviral activity against Influenza A virus.

Sébastien Dilly, Aurelien Fotso Fotso, Nathalie Lejal, Gloria Zedda, Mohamad Chebbo, Fryad Rahman, Simon Companys, Hélène Charlotte Bertrand, Jasmina Vidic, Magali Noiray, Marie-Christine Alessi, Bogdan Tarus, Stephane Quideau, Beatrice Riteau, and Anny SLAMA-SCHWOK

J. Med. Chem., **Just Accepted Manuscript** • DOI: 10.1021/acs.jmedchem.8b00557 • Publication Date (Web): 20 Jul 2018

From naproxen repurposing to naproxen analogues and their antiviral activity against Influenza A virus.

Sébastien Dilly[1]‡, Aurélien Fotso Fotso[2]‡, Nathalie Lejal[3]‡, Gloria Zedda[4]‡, Mohamad Chebbo[2], Fryad Rahman[2], Simon Companys[4], Hélène C. Bertrand[4], Jasmina Vidic[3], Magali Noiray[5], Marie-Christine Alessi[2], Bogdan Tarus[3], Stéphane Quideau[4], Béatrice Riteau[2], Anny Slama-Schwok[1,3]*

1- Gustave Roussy Institute, Paris Saclay University, UMR8200 CNRS, Villejuif, France.

2- Aix Marseille University, INSERM, INRA, NORT, UMR 1260/1062, Marseille, France;

3- Paris Saclay University, UR 892, INRA, Jouy en Josas, France;

4- Bordeaux University, ISM (CNRS-UMR 5255), Talence, France;

5- Paris Sud University, Paris Saclay University, UMS IPSIT - Intermol, Châtenay-Malabry, France;

KEYWORDS: Antiviral, monomeric nucleoprotein, RNA-protein and protein-protein interactions, *in vivo* mice model of intranasal IAV infection, naproxen.

ABSTRACT: The nucleoprotein (NP) of Influenza A virus (IAV) required for IAV replication, is a promising target for new antivirals. We previously identified by *in silico* screening naproxen being a dual inhibitor of NP and cyclooxygenase COX2, thus combining antiviral and anti-inflammatory effects. However, the recently shown strong COX2 antiviral potential makes COX2 inhibition undesirable. Here we designed and synthesized two new series of naproxen analogues called derivatives **2**, **3** and **4** targeting highly conserved residues of the RNA binding groove, stabilizing NP monomer without inhibiting COX2. Derivative **2** presented improved antiviral effects in infected cells compared to that of naproxen, and afforded a total protection of mice against a lethal viral challenge. Derivative **4** also protected infected cells challenged with circulating 2009-pandemic and oseltamivir-resistant H1N1 virus. This improved antiviral effect likely results from derivatives **2** and **4** inhibiting NP-RNA and NP-polymerase acidic subunit PA N-terminal interactions.

Introduction:

Influenza A viruses (IAV) are a societal and economic burden with yet unpredictable bursts. The growing resistance of circulating strains to present amantadine-derivatives and the low (1-3%) resistance to neuraminidase inhibitors urged the development of additional therapeutic options. Various hypotheses have been pursued to overcome resistance. Recent antiviral strategies have focused on internal viral proteins, in particular on the ribonucleoprotein complex [1-6], as detailed below and the non-structural protein-1 NS-1 being a virulence factor [7]. Additional omics studies have identified host cellular factors used by the virus, as several MAP kinases for which targeted inhibitors are available drugs. It is likely that these studies will lead to repurposing of many drugs in the near future.

New therapeutic perspectives have been opened up by targeting conserved viral proteins, as protein of the ribonucleoprotein complex involved in transcription and replication of the virus. The crystal structures of the nucleoprotein (NP) assembled in a trimeric form [8, 9] have highlighted the self-assembly of NP monomers via its tail-loop and hence NP activity could be inhibited by targeting the crucial E339-R416 salt bridge for NP trimer stabilization [10]. High throughput studies have identified nucleozin as a potent inhibitor of the NP that binds at Y52, N309[11, 12], a site shared with antiviral proteins of the MX1 families [13]. Disrupting the interaction of NP and viral RNA was achieved by naproxen that stabilized the NP in a monomeric form [5, 14]. Compound RK424 binds in a small pocket close to the dimer interface and the nuclear expert signal-3 NES3, at a phosphorylation site nearby the naproxen binding site. The residues interacting with RK424 deduced from docking studies were R162, S165, L264, and Y487[15]. Additional protein-protein interactions could be targeted by small molecules inhibitors based on earlier structures of isolated domains of the polymerase subunits [2] and recent structures of the

trimeric polymerase of Influenza A, B and C [4, 16-18-19]. Still, the interactions between NP and the polymerase remain to be characterized to serve as a structural basis for drug design.

In our earlier studies, we have been developing new inhibitors targeting the nucleoprotein by disrupting the interactions between NP and viral RNA. For this, we screened *in silico* for molecules that would stack on Y148, the only aromatic residue in the putative RNA binding groove of NP, stabilized by hydrophobic interactions with the C-terminal, in particular F489, and by electrostatic interactions with nearby arginine residues as R355, R361 or R152. Our first hit was naproxen, a known drug for its anti-inflammatory effect, being a cyclooxygenase (COX2) inhibitor. We showed that naproxen combined antiviral and anti-inflammatory effects by targeting both NP and COX2 [5]. Of note, naproxen also did not promote resistance after eight cell passages when oseltamivir already generated resistance to treatment after 4-5 cell passages [5]. The present work describes the design, *in silico* docking, chemical synthesis, cellular and *in vivo* antiviral effects of a new series of naproxen analogues. We demonstrate that some of these derivatives not only impeded NP-RNA interactions, but also NP-polymerase association.

Results

1- Modeling naproxen analogues by fragment-based drug design:

Derivatives of naproxen were designed to additionally target specific arginine residues of the RNA binding groove of NP besides R361 recognized by naproxen (Figure 1A). To improve their affinity and specificity for NP, addition of an aliphatic or aromatic carboxylate fragment to naproxen led to the first two derivatives **1** and **2**, respectively (Figure 1B, C). The additional

carboxylate fragment aimed at reaching the residues R152/ R150 in addition to R361, while keeping stacking interactions of Y148 and the C-terminal F489 with the aromatic naphthalene core of naproxen. The stability of naproxen derivatives in their binding pocket were investigated through MD simulations of the complex with NP (Table 1). We rapidly discovered that the aliphatic carboxylate fragment of derivative **1** was not optimal in *in vitro* and cellular assays (vide infra). Our previous simulations [5, 6, 20] with derivative **2** showed that Y148 made transient π-π interactions with both the phenyl and naphthalene rings of this derivative leading to some destabilization within the binding site. As Y148 is the only aromatic residue in the RNA binding groove [8] suggested to be important for NP interaction with RNA, we aimed at a better recognition of this residue by designing new naproxen derivatives. We extended the structure of derivative **2** with an aminophenol fragment at either the meta position (derivative **3**, Figure 1D) or the ortho position (derivative **4**, Figure 1E) of the 1,3-benzenedicarboxylate unit. The derivative **3** was designed to donate a hydrogen bond to the hydroxyl group of Y148, and the derivative **4** was designed to target the ring of Y148 through a hydrophobic interaction with the aminophenol ring.

The stabilities of the new derivatives **3** and **4** within their initial putative binding pockets on NP were tested through molecular dynamics (MD) simulations in explicit water and compared to that of derivative **2**. Table 1 and Supplementary Figure 1 compare the interaction energies of the ligands in complex with the nucleoprotein. We expected the following order of stability of the NP-ligand complexes: derivative **4** > derivative **3** > derivative **2** by the free binding energy estimation (Table 1). Docking and MD simulations showed that the binding site of derivative 4 (green) was distant from those of other compounds (Figure 1F). This difference occurred after 30 ns of simulation (Supplementary Figure 1). The carboxylate groups of derivative **4** form tighter

interactions with new arginine residues R150, R152, R156 and R195 (Figure 1E and Table 1) as compared with those involved in binding to derivative **2** involving mainly R152 and R355 (Figure 1C). R152 and R156 were also engaged in π-cation interactions with the naphtalene moiety, thus strongly stabilizing this part of derivative **4**. As expected, the additional aminophenol group of derivative **4** recognized Y148 and R150 through an aromatic and cation-π interactions.

In contrast with derivative **4**, derivative **3** bound at a NP site close to the binding site of derivatives **1** and **2** (Figure 1D). However, a stabilization of the aminophenol group by an stacking with Y148 and a π-cation interaction with R361 induced a rotation of 180° as compared to the orientation observed in naproxen and derivatives **1** and **2** (Figure 1A-C). Derivative 3 forms only a salt bridge with R361 while one carboxylate interacting with the backbone and the side-chain of N149 through hydrogen bonds, thus explaining its lower affinity than that of derivative **4**.

Besides interactions of the naproxen analogue 4 within its binding site, structural changes of the protein are observed upon binding, as previously reported for derivative **2** binding to NP [6]. Clear changes in the oligomerization loop folding back upon its own RNA binding groove, the cavity around E339 where the oligomerization loop protrudes from the next monomer within NP trimer shrinks upon derivative **4** binding to NP, all these changes are consistent with a destabilization of NP trimer and stabilization of NP monomer by derivative **4**. Figure 2A shows that the induced fit observed upon derivative **4** binding to NP resembles the structural changes observed in R416A (Figure 2B), a prototype of monomeric NP with very weak RNA binding

ability[14]. Moreover, the cavity receiving the oligomerization loop (around E339) shrinks by derivative **4** binding to NP in a similar way as that observed in R416A (Figure 2C and D, respectively).

2- Chemical synthesis

*Synthesis of derivative **4*** (12) (see Scheme 1). Derivative **4** (12) was synthesized in ten steps as depicted in Scheme 1. Commercially available 2-nitro-meta-xylene (1) was brominated in 93% yield using molecular bromine and a catalytic amount of powdered iron [21]. The resulting bromo derivative 2 was reduced with iron in the presence of acetic acid to furnish 2,6-dimethyl-4-bromoaniline (3) in 90% yield [22]. This aromatic amine was converted into the corresponding iodo derivative 4 by a Sandmeyer reaction in 60% yield. Oxidation of the two methyl substituents of 4 using potassium permanganate ($KMnO_4$) in a refluxing 1:1 tert-butanol (t-BuOH)/H2O solvent mixture led to the unknown isophthalic acid derivative 5 in 65% yield. Esterification of both carboxylic groups of 5 could not be accomplished by simply using MeOH in the presence of concentrated H_2SO_4. Only a monoester was obtained, so the second carboxylic acid group was esterified using MeI in the presence of K_2CO_3. The diester 6 was then coupled with commercially available 6-methoxy-2-naphthaleneboronic acid (7) under Suzuki conditions [23] to afford the naphthylisophtalate derivative 8 in 47% yield. Coupling of 8 with para-acetamidophenol 9, easily prepared from para-aminophenol [24], was accomplished under Ullmann-type conditions [25], but unfortunately the desired diaryl ether 10 was isolated in only 10% yield. Nevertheless, derivative 4 (12) was finally obtained by complete hydrolysis of 10 in two steps; the hydrolysis of the amide group was performed using 1 N HCl in 1,4-dioxane to

afford 11, which was then saponified using aqueous potassium hydroxide (KOH) in refluxing THF to furnish 12 in 50% yield over the two steps (Scheme 1, see the Supporting Information for details).

*Synthesis of derivative **3*** (20) (see Scheme 2). Derivative **3** (20) was synthesized in seven steps starting from commercially available 4-bromo-2,6-dimethylaniline (13), as shown in Scheme 2. This aromatic amine was quantitatively converted into to the corresponding iodo derivative 14 via a Sandmeyer reaction. Oxidation of its two methyl substituents using potassium permanganate ($KMnO_4$) in a refluxing 1:1 tert-butanol (t-BuOH)/H2O solvent mixture led to the known isophthalic acid derivative 15 [26], which was classically esterified using MeOH in the presence of concentrated H_2SO_4. Coupling between the resulting 5-bromo-2-iodoisophthalate 16 and the commercially available 6-methoxy-2-naphthaleneboronic acid (7) under Suzuki conditions [23] afforded the 2-naphthylisophtalate derivative 17 in 40% yield. Compound 17 was then coupled with para-acetamidophenol 9 under Ullmann-type conditions [25], but again the desired diaryl ether 18 could be isolated in only 10% yield. Derivative 3 (20) was finally obtained by first hydrolyzing the amide group of 18 in quantitative yield using 1 N HCl in 1,4-dioxane, and the resulting free aniline derivative 19 was saponified using aqueous KOH in refluxing THF to furnish 20 in 50% yield, as for derivative **4** (12) (Scheme 2, see the Supporting Information for details).

3- Differential stabilization of monomeric NP by the naproxen analogues

NP contains an oligomerization loop involved in self-association and together with two other flexible loops promotes interactions with RNA of great importance for NP function (see Figure

2). Therefore, we anticipated that a compound stabilizing the monomeric NP would potentially disturb intermolecular interactions, as NP-NP and NP-RNA interactions. We used dynamic light scattering for monitoring the thermal stability of NP by the apparent protein size as a function of temperature. The experimental conditions used for preparation of recombinant NP have been shown to produce NP in a monomeric form (> 80%)[20]. This experiment estimated whether naproxen or the naproxen analogues stabilized monomeric NP against thermal denaturation. The first derivatives of the melting curves considered as the apparent melting temperatures (Tm) of the NP-ligand complexes were used for ranking the relative affinity of compounds to bind NP at 1/1 NP/ compound ratio (Supplementary Figure 2). While naproxen did not stabilize NP, derivatives **2** and **4** stabilized NP (Table 2). The melting of derivative **3**-NP complex showed a biphasic melting profile, thus, the formed complexes were less stable than those formed between NP and derivatives **2** and **4**. Such ranking of naproxen analogues regarding their ability to bind NP (derivative **4** ≥ derivative **2** >> naproxen) was similar from the modeling studies (Figure 1). The biphasic behavior of derivative **3** could be explained by the aminophenol fragment binding tended at destabilizing the naproxen backbone that was not well buried into NP RNA binding groove.

The above models suggested that derivatives **2** and **4** binding to NP likely involved residues of NP also proposed to be important for polymerase assembly and function as C-terminal F489 [27]. Naproxen and derivative **2** binding to NP reduced the flexibility of loop 2 (residues 200-214) and that of a loop close to the C-terminal (residues 429-436) and involved R152 located very close to R150. Since loop 2 residues R204, W207 and R208 [20] and R150 are required for vRNA synthesis [28] and polymerase function [29], we anticipated that the new naproxen derivatives, in particular derivative 4 that interact with R150 would not only impede NP-RNA interactions but also

interfere with polymerase function. We have recently identified a complex between NP and the N-terminal of polymerase acidic subunit PA, away from the endonuclease active site of PA [30]. We investigated whether the naproxen analogues may disrupt the NP-PA(1-27) peptide complex.

We have previously described a pull-down assay based on complex formation between proteins from lysates of IAV-infected cells with the PA (1-27) attached to magnetic beads [30]. A specific complex was observed between PA(1-27) and recombinant NP or NP from the lysate of influenza virus infected cells as revealed by Western blot analysis using a monoclonal antibody against NP (Figure 3A). We then compared naproxen and derivatives for their ability to impede this interaction. Both naproxen and derivative **1** were inefficient in disrupting this interaction. In contrast, derivatives **2**, **3** and **4** efficiently inhibited this interaction as detected by western blots. Of note, NP was likely bound to nucleic acids in WB assay since the cell lysates were not treated for digestion of nucleic acids.

4- SPR experiments

We performed surface plasmon resonance experiments for a quantitative comparison of the relative affinities of naproxen and derivative **2**, as they differ in their ability for NP-PA(1-27) complex disruption (Figure 3A). In these experiments, the biotinylated PA(1-27) peptide was captured onto the chip surface and NP alone or NP with the naproxen or derivative **2** were injected onto the chip. We also tested NP-DNA complexes in the presence of the naproxen analogues. We were unable to replace DNA by RNA as the RNA-complexes stick to the reference surface to a great extent. When NP alone was injected to the chip, a complex NP-PA(1-27) was evidenced.

Addition of derivative **2** (100 nM) to NP largely reduced the signal of the complex (Figure 2B-a). We reproduced the same experiment while replacing derivative **2** by naproxen. Naproxen perturbed NP-PA(1-27) complex less efficiently than derivative **2** did and was unable of NP-DNA-PA(1-27) complex disruption, even at a concentration of 50 µM (Figure **3**B-b,c). In contrast, the NP- PA(1-27) complex formed in the presence of DNA was disrupted by derivative **2** in dose-dependent manner, with an IC50 of about 30 nM (Figure 3B-d). These data are in good agreement with the western blots (Figure 3A).

***5- Cytotoxicity tests*:**

Before testing the antiviral activities of derivatives **2**, **3** and **4**, we performed cell viability tests by MTT and trypan blue tests to verify their cytotoxicity (Figure 4 and Table 2). The naproxen analogues in their salt form were very soluble in buffer. The cytotoxic concentration CC_{50} of derivatives **2**, **3** and **4** were tenfold higher than that of naproxen, being 13 mM and 1.4 mM, respectively (Figure 4).

6- Comparison of the antiviral effects of the naproxen analogues and naproxen in IAV-infected MDCK and A549 cells.

The protection of infected MDCK cells against a viral IAV challenge was tested at two multiplicities of infection, MOI= 10^{-3} after 48 hours and MOI = 2 after 18 hours reflecting conditions of multiple cycles of viral replication, with mild and higher viral load. At low MOI, we determined viral titers whereas at higher MOIs, we measured NP levels by IF, corrected for

cell viability assessed by DAPI measurements. We used both A/WSN/33 (H1N1) (Table 2: MDCK cells) and A/Udorn/72 (H3N2) strains (Table 4, MDCK cells). The latter strain was also applied on A549 cells as summarized in Table 3.

-*Antiviral effect against A/WSN/33 (H1N1)*

At MOI = 2, the dose- response curve of derivative 2 was clearly shifted toward lower concentrations as compared to that of naproxen (Figures 4A,B). The antiviral effect of derivative **2** was similar for the two viral strains, giving IC_{50} about 5 times lower than that for naproxen (Tables 2 and 3). Consequently, the selectivity index (SI) of derivative **2** being 684 increased by ~50 fold as compared to a SI value of 14 for naproxen.

At MOI 10^{-3}, derivative **1** achieved a partial protection of the infected cells and was therefore discarded for further investigation. The IC_{50} values were about one order of magnitude lower for derivatives **2** and **4** than for naproxen, yielding selectivity indexes of 5200 and 9230, respectively, compared to 87 for naproxen (Table 2).

-*Antiviral effect against A/Udorn/72 (H3N2)*:

Tables 2, 3 and 4 showed that the derivatives **2** and **4** presented very similar antiviral effects against H3N2 and H1N1 strains, protecting both MDCK and A549 cells.

-*Antiviral effect against the 2009 pandemic Influenza strain A/Netherlands/602/09*

Figure 5A, B and Table 5 summarize the protection afforded by the derivatives **2**, **3** and **4** against a viral challenge with the pandemic 2009 Influenza A strain. 10 μM of derivatives **2** and **4** significantly protected the MDCK cells while the derivative **3** only slightly protected the cells. Quantification of the IF results presented in Figure 5C, yielded the following order of efficacy:

derivative **4** > derivative **2** > derivative **3**. The selectivity index of derivative **4** reached 17000 as compared to 2600 and 619 for derivatives **2** and **3**, respectively.

- *Antiviral effect against the oseltamivir-resistant strain*

We generated oseltamivir-resistant A/PR/8/34 (H1N1) virus obtained after 4 cell passages as described in the Experimental section. This virus was used to infect MDCK cells and representative IF data are shown in Figure 6A-B; quantification is shown in the insert of panel B. Treatment with increasing concentrations of derivatives 2 and 3 afforded a better protection of the cells, in contrast with 2µM of derivative **4** being already protective. Oseltamivir could not protect these cells against this oseltamivir -resistant strain as shown in panel C, while oseltamivir had a clear antiviral effect in oseltamivir -sensitive A/PR/8/34 (H1N1). Table 6 summarizes the antiviral effects of derivatives **2**, **3** and **4**. Note that derivative **4** is equally efficient in the pandemic and oseltamivir -resistant Influenza A strains within experimental error.

7- Loss of the anti-COX2 activity of naproxen by affording more selective antiviral compounds.

Naproxen is an anti-inflammatory drug which analgesic and anti-inflammatory effects are dependent on the extent and duration of cyclo-oxygenase-2 (COX2) inhibition in the spinal cord and inflammatory sites. However, the simultaneous inhibition of COX2 in the vasculature increases the risk of hypertension and heart failure while lowering doses cannot avoid the cardiovascular risk of naproxen in high-risk CV patients [31]. Therefore, it is desirable for an increased safety of naproxen analogues to avoid COX2 inhibition. Moreover, the infection with influenza A viruses (IAV) provokes activation of cellular defense mechanisms contributing to

the innate immune and inflammatory response. In this process the cyclooxygenase-2 (COX2) plays an important role in the induction of prostaglandin-dependent inflammation. While it has been reported that COX2 is induced upon IAV infection, inhibition of COX2 expression by IAV viruses strongly suggests that COX2 inhibition is undesirable to fight against IAV [32].

We tested whether COX2 levels were increased in IAV infected cells compared to uninfected cells and whether naproxen and derivative 2 would reduce COX2 levels. Figure 7 shows an increase of COX2 induced by IAV. This increased COX2 level was significantly reduced by addition of 300 μM naproxen, a concentration at which the viral titer is reduced by two orders of magnitude in infected cells[5]. In contrast, derivatives **2** or **4** (100 μM) did not inhibit COX2.

For the below *in vivo* studies, we used derivative **2** as a prototype of the naproxen analogues and compared its effect with naproxen treatment of IAV-infected mice.

8- Derivative 2 protected mice more efficiently than naproxen against a viral challenge.

The antiviral activity of derivative **2** was then evaluated in a mice model of Influenza A/PR/8/34 (H1N1) infection (500 pfu/mouse), infected at day 0. The mice were treated by intraperitoneally administration of naproxen or derivative **2** or oseltamivir or saline buffer shortly after infection (5-10 minutes), and once a day during the next two days, at days 1 and 2. The protection afforded by derivative **2** administered at 1 or 8 mg/mouse/day (50 or 400 mg/kg, respectively) was compared with naproxen treatment used at 1mg/day. The survival curves showed a dose-dependent protection when the mice were treated with derivative **2** (Figure 8A). The survival rates at day 12 post-inoculation reached 70 % when treated with 1 mg/day of derivative **2** while only 20% of the mice survived after naproxen treatment. A complete protection was achieved by

treating the mice with derivative **2** at 8 mg/day or with oseltamivir. Consistently, when treated with only 1 mg of derivative **2**, the mice could recover up to 95% of their initial weight while naproxen could only stabilize their weight loss to 85% of their initial weight (Figure 8B). Amazingly, the mice completely recovered from a mild (5%) weight loss upon treatment with 8mg/day of derivative **2**. The mice treated with derivative **2** (8mg) were more protected against weight loss than with oseltamivir treatment during the first days of infection, while all mice survived under both treatments.

To further corroborate the observed antiviral effect deduced from the survival and body weight loss curves, we determined the viral titers in the BAL at the third day post-inoculation. In infected vehicle-treated mice, the viral titer reached 2 x 10^7pfu/ml. In mice treated with naproxen or derivative **2** (1 mg/day), the viral titer was reduced by 2 and 6 folds. Higher derivative **2** concentration (8 mg/day) decreased the viral titer by two orders of magnitude (120 folds). In the same conditions, oseltamivir reduced the viral titer by 260 folds, within experimental error a similar protection than that of derivative **2**.

Discussion:

NP plays a pleiotropic role in the RNP function, stabilizing both cRNA and vRNA, disrupting RNA secondary structures facilitating transcription, supporting elongation of nascent transcripts during replication. NP is a highly abundant and conserved viral protein, with no equivalent protein in the host cell transcription/ replication machinery. When combined, these arguments strongly support that NP is a good target for new antivirals. From these essential roles of NP in viral functions, it could be anticipated from an inhibitor of NP to interfere with RNP function [33].

-Stabilizing both NP C-terminal and nearby residues of the RNA binding groove for targeting both NP and the polymerase ie PA N-terminal. The interaction modes of the NP with polymerase subunits still require insight at the molecular level. The strength of molecular modeling and protein-protein docking is to suggest models based on very solid crystal structures of each NP and polymerase component to be validated in experimental studies. Interactions of NP with PB1 and PB2 [4], NP and the C-terminus of PA were observed. Electron microscopy showed a rearrangement of the polymerase, in particular in the PA subunit [1, 4, 11] in these NP-PA interactions, a phenomenon confirmed by our docking studies [30]. We also identified a complex between NP and PA N-terminal by docking, further supported by experimental tests *in vitro* and in the lysate of infected cells. This complex could be a target for antiviral drug [30].

We went here one step further in targeting not only the NP-RNA interactions as demonstrated for naproxen but also protein-protein interaction. To do so, we extended naproxen by fragment-based drug design [6], to stabilizing Y148 and the C-terminal aromatic residues F489, F488 by stacking interactions with their aromatic backbone and reaching nearby RNA binding groove residues R152 and R355 in addition to R361 recognized by naproxen. Of note, mutation of all these residues was found to be lethal, since they could not be rescued[34]. Preliminary attempts to extend the methoxy group of naproxen were destabilizing compared to naproxen binding, likely because of the presence of a "bump" formed by Y487, F338 from one side, F488 from the other side that would not favor binding of short polar fragments (data not shown). This hydrophobic region was proposed to stabilize the biphenyl group of RK424 (via Y487 or F488) bearing a naproxen-like quinoline core, a compound proposed to bind NP at a close-by site from the binding site of naproxen demonstrated by point mutations [15]. Because of NP flexibility, the binding of derivative **2** induced changes in the binding pocket of the tail loop, affecting in

particular E339, Y487 and S165, and reduced the flexibility of loop 1 (residues 73–90) and loop 2 (residues 200–214) and a C-terminal linker (residues 428-438) [6]. As S165 is a residue that can be phosphorylated, such induced fit by derivative **2** or derivative **4** binding may affect NP post-translational modifications and likely other protein-NP interactions[14, 35]. Because the RNA binding groove and C-terminal residues of NP stabilized by derivatives **2**, **3** and **4** are participating to NP-PA – N-terminal interactions, we anticipated that these naproxen analogues would disrupt the complex. We identified this complex in the supernatant of infected cells; it was disrupted by derivative **2**, **3** and **4** while naproxen and derivative **1** were inefficient in this competing binding, in agreement with our expected interaction site for NP-PA N-terminal complex. Additionally, derivative **1** had a biphasic behavior in competition studies, suggesting more than one binding site. The SPR data confirmed and quantified the specific disruption of the complex with PA(1-27) by derivative **2** with an IC50 of 30 nM. The ten-fold decrease in IC50 value of derivative **2** for NP was consistent with a more efficient competition for disrupting RNA binding to NP than that observed for naproxen [5, 6].

Conclusions:

- *Suitable predicted drug-like profile of the naproxen analogues.* The new naproxen analogues present a relatively low molecular weight, a good solubility in aqueous solution, properties of many drug-like compounds. To assess more precisely the predicted pharmacokinetics and drug-like profile of the naproxen derivatives, we used different relevant drug-like filters (Table 7). First, the bioavailability radar calculated by the free web tool SwissADME [36] indicated that the two negative charges of the carboxylate moieties of derivatives **2**, **3** and **4** does not really impact

the bioavailability profile of the compounds in comparison with naproxen, with 5 out of 6 physico-chemical parameters important for the bioavailability are still present the favorable pink region. We also applied the Lipinski's rules[37] and a bioavailability score developed by Abbot laboratories[38]. According to the first filter, no violation is observed for the different derivatives, indicating that they have high predicted probability to be an oral drug. The second filter shows for all compounds having a probability of 56 % and at least 10% oral bioavailability in rat or measurable Caco-2 permeability. Then, we used the GI absorption predictor calculated by the BOILED-Egg model, a model for passive human gastrointestinal that indicates a high score of absorption for all compounds[39]. Finally, we employed a P-glycoprotein (P-gp) substrate filter to evaluate the capacity of the compounds to undergo efflux through biological membrane [40]. None of the compounds were predicted to be substrates of the P-gp protein. In conclusion, the results of these drug-like filters indicate that the structures of the naproxen derivatives, especially the presence of two carboxylic acids, are not critical for the predicted pharmacokinetics profile of the compounds. Another possible drawback is the presence of an aniline moiety in the structure of the derivative **4**. Indeed, this chemical group is known to present liver cytotoxicity. To overcome this possibility, the amino group could be removed without affecting the activity of the compound since it does not participate in the molecular recognition by the NP (Figure 1E). Indeed, the recognition is mainly driven by the phenyl moiety involved in π-π stacking interactions with Y148 and cation-π interactions with R150.

Improved antiviral efficacy of the naproxen analogues. The higher affinity of derivatives **2**, **3** and **4** for NP than that of naproxen was at the expense of a lower affinity for COX2. Although it is desirable to reduce airway inflammation induced by Influenza A virus, naproxen inhibition of COX2 could be associated with an increased cardiovascular risk. Therefore, the lack of

significant inhibition of COX2 levels by derivative **2** might increase the cardiovascular safety, in addition with antiviral properties.

Accordingly, when compared to naproxen, derivative **2** presented more efficiently protected cells against a viral challenge with two viral stains, H1N1 (Influenza A/ WSN/33 and A/PR8/34) and H3N2 (Influenza A/Udorn/72). A 5 to ten- fold decrease in the relative efficacy in the antiviral effect combined with a higher CC_{50} value makes derivative **2** an interesting antiviral lead candidate (Tables 2 & 3). This increase of efficacy was also observed in *in vivo* experiments: derivative **2** could totally protect mice from a viral challenge. This correlated with a two orders of magnitude decrease of the pulmonary viral titer.

Moreover, derivative **4** was equally protecting MDCK cells against viral challenges with pandemic A/Netherlands/602/09 strain, A/WSN/33 and oseltamivir- resistant A/PR/8/34 (H1N1) virus, with IC50 being 1.0 ± 0.2 μM, 1.3 ± 0.2 μM, 0.7 ± 0.1 μM, respectively at MOI 10^{-3} with SI values in the range 10000 - 20000. We emphasize that derivative **4** was more potent than derivative **2**, for which the following IC50 were obtained 8.8 ± 2.5 μM, 2.9 ± 0.4μM, 2.0 ± 0.5 μM and 5 ± 3 μM for A/Netherlands/602/09 strain, A/WSN/33, A/Udorn/72 (H3N2) and oseltamivir-resistant A/PR/8/34 (H1N1), respectively.

-Interest in combining antiviral and anti-inflammatory effects in severe cases of IAV infection. Previous combination regimen has shown that a bi-therapy is more effective with drugs addressed to two targets as for example HA and NA proteins[2, 3] than two drugs targeting a single protein. Recently, a clinical trial enrolling 217 patients with influenza A (H3N2) showed the improved efficacy of a combined regimen of naproxen, oseltamivir and clarithromycin than

oseltamivir alone in reducing both 30- and 90-day patient mortality and length of their hospital stay [41].

Our present results suggest that the improved efficacy of the naproxen analogues may result from disrupting the interactions involving two viral proteins, more efficient than inhibition of a single viral target by disrupting NP-RNA interactions. While a bi-therapy directed against two viral targets might be appropriate, a (bi or tri-) therapy combining antiviral and anti-inflammatory action may afford a better protection, in particular in severed case of IAV infection or in patients with allergic background (asthma) or immunocompromised status. Such therapies could combine molecules such as derivatives **2** or **4** along with antagonists of receptors promoting the harmful lung inflammation during influenza, such as the formyl-peptide receptor-2 or with inhibitors of NADPH oxidases 2 and 4 [42-45]. Further work along these lines is in progress in our laboratories.

Experimental section

Molecular modelling: Naproxen was selected through virtual screening as described before [5]. The 3D crystal structure of NP monomeric form (PDB ID: 2IQH), was used as target throughout the virtual screening in a volume centered on Y148. The MD simulations were carried out following a protocol detailed elsewhere [5]. The program NAMD [46] with the CHARMM27 force field [47] was employed to perform the MD simulations. The NP-naproxen analogues complex was centered in a cubic cell of pre-equilibrated TIP3P water model [48]. The system was electrostatically neutralized and set to an ionic strength of 0.15 M by adding sodium and chloride ions. The electrostatic interactions were calculated using the particle mesh Ewald summation algorithm [49]. The equations of motion were iterated using the velocity Verlet integrator with a

time step of 2 fs. An initial step of system energy minimization was followed by heating to 300 K. Molecular dynamics simulation in NVE and NPT ensemble were further employed to equilibrate the system and for production run. Trajectories of 40 ns were produced for the NP-derivative **2**, **3** and **4** complexes. For each trajectory, the displacement of the ligands was studied by RMSD calculation. The structures with a close position (RMSD < 1 Å) were then grouped in the same cluster. The representative structure (ie with the smallest average RMSD from all other structures of the cluster) of the largest cluster of each complex was selected and then used for an estimation of the free binding energy using the software Discovery Studio version 2016.

Estimation of the cavity in which the oligomerization loop inserts: the generation of the cavities for the NP-derivative **4** complex, NP alone and the mutated R416A NP was carried out using the cavity detection algorithm implemented in Discovery Studio version 2016 [50].

Drug-like properties of the naproxen analogues: the evaluation of six physicochemical properties (lipophilicity, size, polarity, solubility, flexibility and saturation) for a rapid appraisal of drug-likeness was assessed according to [36].

Chemical synthesis:

Solvents were freshly distilled before use. ^{1}H and ^{13}C NMR spectra were recorded on a Bruker Avance 300 using solvent residuals as internal references. Melting points (MP, uncorrected) were determined on a Büchi Melting Point B-540. TLC analysis was carried out on silica gel (Merck 60F-254) with visualization at 254 and 365 nm. Preparative flash chromatography was carried out with Merck silica gel (Si 60, 40-63 μm). IR spectra were recorded with a FT-IR PerkinElmer Spectrum 100 spectrometer. Mass spectrometry low resolution data (LRMS) and high resolution data (HRMS) were obtained from the Centre d'Etudes Structurales et d'Analyses

des Molécules Organiques (CESAMO), Université de Bordeaux. The HPLC analysis was performed with the following equipment and experimental conditions: HPLC Thermo Separation Products Spectra SYSTEM (ThermoFisher), Software: ChromQuest, Isocratic elution: 50% acetonitrile / 50% water + 0,1% formic acid by volume, Flow: 1,2 mL/min, Column: Pursuit 5 C18 250 x 4,6 mm, Pump: Spectra SYSTEM P1000XR, Detector: Spectra SYSTEM UV6000LP. All naproxen derivatives had a purity ≥ 95%. The purity percentages of the two newly synthesized and tested compounds have been determined by HPLC analysis to be 97% and 95%. The details of the HPLC and high resolution ^{1}H and ^{13}C NMR data are provided in the Supporting Information.

The naproxen analogues are protected by a patent WO2012143141 (PCT/EP2012/001720 and US patent US14112987, grant US9783482B2, application US20180028478A1)[51].

Reagents: Reagents and chemicals for chemical synthesis were purchased from Sigma-Aldrich. NP primary monoclonal antibody (sc101352) and monoclonal antibody anti-COX2 sc-376861 were purchased from Santa Cruz Biotechnology. Oligonucleotides: Biotinylated (5' end) DNA fragments were purchased from Dharmacon (Thermo-Fischer, France) with HPLC purification; the following sequences were used: Flu1: 5' TTT GTT ACA CAC ACA CAC GCT GTG 3'. The peptide PA(1-27) and a scramble peptide were purchased from Gencust (Luxemburg) at a purification level over 95%. HPLC-purified oligonucleotides were purchased from Eurofins and MGW.

Peptide	Sequence	Length

PA(1-27)	Biot GSGS MED FVR QCF NPM IVE LAE KAM KEY GED	31
Scramble	Biot- GSGS MAI EKI SEI QRG SVF VDR LNV VET ISP DRR GQ	36

The Ni magnetic beads (Pure proteome) were purchased from Millipore. Naproxen, NaCl, Tris buffer, guanidinium chloride, NaOH were from Sigma, MEM (minimal essential medium) media from Lonza (Cologne, Germany). Derivative 2 was synthesized as previously described [6].

Virus Madin–Darby canine kidney (MDCK) cells were obtained from the American Type Culture Collection. The influenza viruses A/PR/8/34 (H1N1), A/Udorn/72 (H3N2) were grown in 8 days old embryonated hens'eggs and titered in MDCK cells. A/WSN/33 (H1N1) was produced by reverse genetics: the 12 plasmids from a reverse genetics system were used as described previously (32) to generate a recombinant virus of the influenza A/WSN/33 strain. Briefly, 293T cells were transfected with eight plasmids encoding the individual vRNA segments of influenza A/WSN/33 (H1N1) virus from a truncated human polymerase I promoter and four expression plasmids encoding the corresponding subunits of the viral polymerase and the nucleoprotein. The generated wild type (WT) virus was amplified on Madin-Darby canine kidney cells and titrated by plaque assays. MDCK cells were cultured in minimal essential medium (MEM, Sigma) containing 0.2% $NaHCO_3$ (Sigma), MEM amino acids (Gibco), MEM vitamins (Gibco), PSG, and 5% Newborn Calf Serum (ICN Biochem).

The Pandemic *A/Netherlands*/602/09 strain was a gift from Dr GF Rimmelzwaan, Research Center for Emerging Infections and Zoonoses, University of Veterinary Medicine, Hannover Bünteweg 17, 30559 Hannover, Germany.

– Production of oseltamivir-resistant PR8 virus: In a 6-well plate, 1.5×10^6 MDCK cells were added per well in DMEM 10% FBS medium. After 24 hours of incubation, the cells were infected with PR8 virus at MOI of 10^{-3} in the presence of 500 μM oseltamivir in DMEM without FBS. After 24 hours of incubation, the supernatant was taken and the virus was titrated. Then this virus was used to repeat the same experience. After 4 cell passages, the virus became resistant to oseltamivir.

Protein expression and purification of wt NP: Protein expression was performed as described [20] with modifications of the purification protocol by affinity chromatography using Ni magnetic beads (Pure proteome, Millipore) and performed as recommended by the manufacturer, followed by extensive dialysis at 50 mM NaCl, 20 mM Tris buffer at pH= 7.5. In these conditions, NP is over >80% monomer. After purification, the protein concentration was determined by the extinction coefficient $\varepsilon = 56200\ M^{-1}.cm^{-1}$ at 280 nm.

Dynamic light scattering: The measurements were performed on a Malvern Zetasizer nanoS apparatus thermostated at 20°C. The size distribution was calibrated with latex particles of 65 and 200 nm radii. The scattering intensity data were processed using the instrumental software to obtain the hydrodynamic diameter (Dh) and the size distribution of scatterers in each sample. A total of 10 scans with an overall duration of 5 min were obtained for each sample and time point. All data were analyzed in triplicate. Melting curves were obtained by recording the mean size as a function of temperature in the range 20 to 70 to 80°C, using a temperature gradient of 1°C/ minute The Tm value was obtained from the maximum of the first derivative curve. The protein concentrations usually were in the range of 5 to 15 μM. The samples for dynamic light scattering were prepared in 20 mM Tris buffer at pH = 7.4 with 50 mM NaCl.

Surface plasmon resonance experiments: The binding kinetics were performed on a Biacore T100 apparatus using streptavidin coated sensor-chips (SA, GE Heathcare). Capture of the biotinylated peptide on the streptavidin coated sensorchip was carried out in running buffer. The SPR kinetic measurements were performed in 20 mM Tris-HCl buffer, pH=7.4 at 25 °C, containing 300 mM NaCl and 0.005% P20. Regeneration was performed by injecting guanidium chloride during 30 sec, followed by two 30 seconds pulses of NaOH 10 mM. The peptides stock solutions at a concentration of 250 μM were dissolved in water containing 1% DMF. The peptides diluted in the running buffer at a concentration of 2.5 nM were injected for attachment to the surface using the manufacturer protocol usually at a density of about 1500 RU. The NP protein was injected at concentrations of 12 to 2500 nM in the presence or absence of naproxen analogues, up to 50μM in some experiments. Measurements were conducted at 25°C and samples were injected at 30 μl/min flow rate. The scramble and PA(1-27) peptides were attached to the surface of the same chip at similar RU. To normalize SPR signal intensities, we probed known interactions between a peptide P1 from N-terminal of PB2 and a peptide P4 from PB1 C-terminal 34 of similar size than that of PA(1-27) as a positive control. The signal that corresponded to the P1-P4 complex observed at saturation when P4 (MW 4185 Da) was injected on immobilized P1 in the running buffer containing 300 mM NaCl and 0.005% P20 was 25 RU. The signal of NP is expected to be proportional to the ratio of the molecular weights of NP versus P4. NP adopts mainly a trimeric/ tetrameric form with an apparent MW of 197 Kda. Thus, the signal at saturation for NP-PA(1-27) complex formation is expected to be 25 x 197 170/ 4185 = 1175 RU using P1-P4 interaction as a reference. When 1.6 μM NP was injected over immobilized PA(1-27) surface, the SPR signal corresponding to the NP - PA(1-27) complex formation was found to be 1200 RU, in good accordance with a calculated Rmax.

Cell culture and infection: Madin-Darby canine kidney cells (MDCK) were purchased from the American Type Culture Collection (Manasses, VA) and grown in MEM medium supplemented with 10% fetal calf serum (FCS), 2 mM glutamine, and antibiotics. Cells were cultured at 37°C in a 5% CO2 incubator. Before infection, cells were washed with FCS-free medium and incubated with A/WSN/1933 (H1N1) virus at multiplicity of infection of 2. Infected cells were then incubated at 37°C until collection at 18 hours post-infection. For WB, collected cell pellets were homogenized in PBS containing anti-proteases (Roche), 1:1 volume. Both pellets and supernatants were frozen at -80°C until WB probing. For measurements of NP levels by immunofluorescence, the cells were labeled with a monoclonal antibody (sc101352).

Cell viability assay by MTT assay: A549 or MDCK cells ($3.2x10^5$ cells / well) were cultured in 12-well plates at 37 °C for 1 day in MEM without Fetal Calf Serum. Serial dilutions of naproxen (1μM – 10 mM) were added to the cells that were further incubated at 37°C for 24, 48 hours. Same culture conditions were used for the antiviral tests and toxicity measurements. MTT analysis was performed based on the standard method. The absorbance was measured at 550 nm with subtraction of the blank value at 650 nm using a Plate Reader (PerkinElmer). The presence of naproxen or its derivatives in the supernatants did not affect the readings within experimental error. The data at 24 h were best fitted by a dose-response curve The toxicity data (2 μM – 30 mM) were fitted with a dose-response curve (Origin, v8.5 software) to determine the CC_{50}.

Cell viability by Trypan blue dye exclusion method: MDCK cell cultures (3.2×10^5 cells /well) were grown in 12-well tissue culture plates. After a 24 h period of incubation, the same procedure for the cytotoxicity assay described above was followed. After 48 h the supernatant was removed, cells were washed and trypsinized, and Trypan blue dye aqueous solution was added to a cell suspension. Viable and dead cells were counted with a phase contrast microscope.

Pulldown assays: Infected MDCK cells were harvested and resuspended in ice-cold PBS buffer supplemented with a complete protease inhibitor cocktail (Roche). After addition of NP40 surfactant (0.5%), the cells were lysed by freezing at -80°C. For pulldown assays streptavidin-coated magnetic beads, SA-MBs, (Dynabeads M-280 Streptavidin, Invitrogen) were incubated with 250μM PA(1-27) in PBS for 30 min at room temperature. PA(1-27)-SA-MBs were separated with a magnet and washed in PBS. The beads were resuspended in the lysates of infected cells for 18 hours at 4°C. The beads were extensively washed with PBS buffer, boiled in Laemmli sample buffer, and analyzed by SDS-PAGE or immunoblotting. Negative controls were performed by incubating PA(1-27)-SA-MBs with lysates of non-infected MDCK cells, or incubated beads carrying no peptide (SA-MB), or carrying a biotinylated scramble peptide (PScr-SA-MB), with lysis of infected cells.

Immunoblotting: Proteins were eluted from SA-MB in Laemmli buffer at 95°C and subjected to SDS-PAGE. Then, proteins were transferred to nitrocellulose membranes. The membranes were incubated in a blocking solution (PBS–0.1% Tween 20 with 5% nonfat milk) for 3 h. The blots were rinsed with PBS–0.1% (vol/vol) Tween 20 and incubated overnight at 4°C with primary anti-NP monoclonal antibody (Santa Cruz Biotech). The membranes were rinsed and incubated with the anti-mouse horseradish peroxidase (HRP)-conjugated secondary antibody. Immunodetection was performed using the Clarity Western ECL substrate (Bio-Rad).

Antiviral Effect: MDCK or A549 cells (0.32×10^6 cells / well) were cultured in 5% CO_2 for 24 hours to 80% confluence as described above without Fetal Calf Serum. Serum-starved A549 cells or MDCK cells were infected with A/WSN/33 virus at 10^{-3} MOI (multi cycle growth assay) and naproxen or naproxen analogues (0.1 - 500 μM) or vehicle were added to the cells immediately after virus adsorption. Some experiments were also performed at higher multiplicity

of infection MOI = 2 during 18 hours or by replacing Influenza/A/WSN/33 (H1N1) by A/Udorn/72 (H3N2). Viral titers of the clarified cell supernatants were determined by plaque assay using crystal violet read-out at different times as indicated. The viral load was also measured by the level of viral NP (MOI =2) by immunofluorescence using an NP antibody. The experiments were carried out in triplicate and repeated at least twice for confirmation. The IC_{50} was determined by fitting the data to a dose –response curve (Origin version 8.5). In addition, the same method used to evaluate cell viability as described above was followed to determine the CC50 by MTT tests.

MDCK cells (0.32×10^6 cells / well) were cultured in 5% CO_2 for 24 hours to 80% confluence without Fetal Calf Serum. Serum-starved MDCK cells were infected with the 2009 pandemic strain or Oseltamivir-resistant PR8 virus at MOI 10^{-3} during 48 hours. Immediately after infection, the cells were treated or not with the naproxen analogues and used in the concentration range of 2-200 μM. After fixation and treatment with triton, the cells were labeled with a monoclonal NP antibody overnight and labeled with a secondary red antibody. The viral load was assessed by the level of viral NP by immunofluorescence. The experiments were carried out in triplicate and repeated at least twice for confirmation. The NP and DAPI levels were quantified using Image J by determining the raw intensity in each cell subtracted by the raw intensity of the background near the cell. The results were averaged on 10-20 cells. The NP levels in treated cells by derivatives 2, 3 or 4 compared to untreated cells were tested for statistical relevance by ANOVA tests. All statistical analyses were performed using GraphPad Prism.

Determination of COX2 levels by IF: A549 cells were washed twice in DMEM without phenol red and the derivatives were added to the cells and incubated for 30 minutes. Then, viral

inoculum at 5x 10^8 pfu/ml was added to the cells (MOI 2). Alternatively, the cells were activated by 100 µM γ-ATP for one hour in the presence or absence of the derivatives. The cell supernatants were removed, the cells fixed with 3% PFA in PBS for 15 minutes, washed twice and permeabilized with 0.1% triton in PBS + 3% BSA, incubated 15 minutes, rinsed twice and labeled with the primary antibody anti COX2 (ab15191) overnight, then washed twice and labeled with Alexa 647 secondary antibody.

In vivo experiments: Five to six-week-old female C57BL/6J mice (Charles Rivers) were anesthetized with Ketamine/ Xylazine (43/5 mg/kg) and inoculated intranasally with 20 µl of a solution containing A/PR/8/34 virus (500 PFU). Five to ten minutes after virus inoculation, the mice were treated once a day at days 0, 1 and 2. Five mice groups, 10 mice in each group, were treated intraperitoneally: serum, naproxen 1mg/day; derivative **2** at doses of 1, 4 and 8 mg/day. Survival rates and loss of body weight were scored daily. Twenty percent weight loss was used as the end point in the mortality curve following the European Ethics committee recommendations. At the end of the experiment, mice were sacrificed by cervical dislocation. For assessing virus replication, broncho-alveolar lavage (BAL) was harvested from the sacrificed mice, and infectious virus titers were determined by plaque assay. Tamiflu obtained from a pharmacy (0.2 mg dissolved in PBS) was used as a positive control. The protocol was approved by the committee of animal experiments of the Faculty of Marseille la Timone (number: G130555). All animal experiments were also carried out under the authority of a license issued by "la direction des services Vétérinaires" (accreditation 693881479). All statistical analyses were performed using GraphPad Prism. To assess viral replication, we used the Mann-Whitney test. The survival curves were analyzed with the Rank test (Mantel-Cox). The analysis of

variance ANOVA one-way and t-tests were used for statistical analysis. Results were considered statistically significant at $p < 0.05$ (*).

Statistical analysis: All data were presented as means ± standard deviation. Statistical analysis was performed using the one-way ANOVA test with the following significances: * $P < 0.05$ versus control, ** $P < 0.01$ vs control, *** $P < 0.001$.

Ancillary Information:

- Supplementary Figures

- Chemical synthesis of derivative **4** and characterization of all intermediates in the synthesis (NMR, mass)

- Chemical synthesis of derivative **3** and characterization of all intermediates in the synthesis (NMR, mass)

- HPLC Analysis of derivatives **3** and **4**

-Structures of the modeled NP-ligand complexes based on the PDB 2IQH are provided as PDB files

- Molecular Formula Strings-Structures of the modeled NP-ligand complexes based on the PDB 2IQH are provided as PDB files

- Molecular Formula Strings

Acknowledgements: This work was supported by the French agency for research (ANR) for funding (RNAP-IAV, ANR-14-CE09-017-02 to A.S.). This work was granted access to the

CINES resources Occigen made by GENCI (Grand Equipment National de Calcul Intensif) under the grant AP010710343 attributed to S.D. We thank Yannick Boursin, Prof. Daniel Gautheret, and the Bioinformatics core of Gustave Roussy for granting access to the cluster Cigogne.

Abbreviations: DLS: dynamic light scattering; IAV: Influenza A virus; MDCK: Madin-Darby canine kidney cells; MOI: Multiplicity of Infection, NP: nucleoprotein, PA: polymerase acidic subunit; SI: selectivity index; SPR: surface plasmon resonance.

Corresponding Author: * Correspondence should be addressed to Dr Anny Slama-Schwok, UMR CNRS 8200, Institut Gustave Roussy, email: anny.schwok@gmail.com **and** anny.slama-schwok@gustaveroussy.fr**.**

Author Contributions: ‡: SD, AFF, NL and GZ are first co-authors and contributed equally. NL, MC, FR performed cellular experiments, JV, MN and ASS performed and analyzed SPR experiments, SD, BT and ASS performed drug design and BT run MD simulations, BR designed and AFF performed *in vivo* experiments, SQ designed and GZ, SC, HCB performed chemical synthesis, The manuscript was written by ASS through contributions of all authors. All authors have given approval to the final version of the manuscript.

Funding information: This work was supported by a grant from the Agence Nationale de la Recherche RNAP-IAV ANR-14-CE09-0017 to ASS.

REFERENCES

1. Yen, H. L. Current and novel antiviral strategies for influenza infection. *Curr Opin Virol* **2016,** 18, 126-134.

2. Monod, A.; Swale, C.; Tarus, B.; Tissot, A.; Delmas, B.; Ruigrok, R. W.; Crepin, T.; Slama-Schwok, A. Learning from structure-based drug design and new antivirals targeting the ribonucleoprotein complex for the treatment of influenza. *Expert Opin Drug Discov* **2015,** 10, 345-371.

3. McKimm-Breschkin, J. L.; Fry, A. M. Meeting report: 4th ISIRV antiviral group conference: Novel antiviral therapies for influenza and other respiratory viruses. *Antiviral Res* **2016,** 129, 21-38.

4. Stevaert, A.; Naesens, L. The influenza virus polymerase complex: an update on its structure, functions, and significance for antiviral drug design. *Med Res Rev* **2016,** *36*, 1127-1173.

5. Lejal, N.; Tarus, B.; Bouguyon, E.; Chenavas, S.; Bertho, N.; Delmas, B.; Ruigrok, R. W.; Di Primo, C.; Slama-Schwok, A. Structure-based discovery of the novel antiviral properties of naproxen against the nucleoprotein of influenza A virus. *Antimicrob Agents Chemother* **2013,** *57*, 2231-2242.

6. Tarus, B.; Bertrand, H.; Zedda, G.; Di Primo, C.; Quideau, S.; Slama-Schwok, A. Structure-based design of novel naproxen derivatives targeting monomeric nucleoprotein of Influenza A virus. *J Biomol Struct Dyn* **2015,** *33*, 1899-1912.

7. Engel, D. A. The influenza virus NS1 protein as a therapeutic target. *Antiviral Res* **2013,** *99*, 409-416.

8. Ye, Q.; Krug, R. M.; Tao, Y. J. The mechanism by which influenza A virus nucleoprotein forms oligomers and binds RNA. *Nature* **2006,** *444*, 1078-1082.

9. Ng, A. K.; Zhang, H.; Tan, K.; Li, Z.; Liu, J. H.; Chan, P. K.; Li, S. M.; Chan, W. Y.; Au, S. W.; Joachimiak, A.; Walz, T.; Wang, J. H.; Shaw, P. C. Structure of the influenza virus A H5N1 nucleoprotein: implications for RNA binding, oligomerization, and vaccine design. *FASEB J* **2008,** *22*, 3638-3647.

10. Shen, Y. F.; Chen, Y. H.; Chu, S. Y.; Lin, M. I.; Hsu, H. T.; Wu, P. Y.; Wu, C. J.; Liu, H. W.; Lin, F. Y.; Lin, G.; Hsu, P. H.; Yang, A. S.; Cheng, Y. S.; Wu, Y. T.; Wong, C. H.; Tsai, M. D. E339...R416 salt bridge of nucleoprotein as a feasible target for influenza virus inhibitors. *Proc Natl Acad Sci U S A* **2011,** *108*, 16515-16520.

11. Gerritz, S. W.; Cianci, C.; Kim, S.; Pearce, B. C.; Deminie, C.; Discotto, L.; McAuliffe, B.; Minassian, B. F.; Shi, S.; Zhu, S.; Zhai, W.; Pendri, A.; Li, G.; Poss, M. A.; Edavettal, S.; McDonnell, P. A.; Lewis, H. A.; Maskos, K.; Mortl, M.; Kiefersauer, R.; Steinbacher, S.; Baldwin, E. T.; Metzler, W.; Bryson, J.; Healy, M. D.; Philip, T.; Zoeckler, M.; Schartman, R.; Sinz, M.; Leyva-Grado, V. H.; Hoffmann, H. H.; Langley, D. R.; Meanwell, N. A.; Krystal, M. Inhibition of influenza virus replication via small molecules that induce the formation of higher-order nucleoprotein oligomers. *Proc Natl Acad Sci U S A* **2011,** *108*, 15366-15371.

12. Kao, R. Y.; Yang, D.; Lau, L. S.; Tsui, W. H.; Hu, L.; Dai, J.; Chan, M. P.; Chan, C. M.; Wang, P.; Zheng, B. J.; Sun, J.; Huang, J. D.; Madar, J.; Chen, G.; Chen, H.; Guan, Y.; Yuen, K. Y. Identification of influenza A nucleoprotein as an antiviral target. *Nat Biotechnol* **2010,** *28*, 600-605.

13. Zimmermann, P.; Manz, B.; Haller, O.; Schwemmle, M.; Kochs, G. The viral nucleoprotein determines Mx sensitivity of influenza A viruses. *J Virol* **2011,** *85*, 8133-8140.

14. Chenavas, S.; Estrozi, L. F.; Slama-Schwok, A.; Delmas, B.; Di Primo, C.; Baudin, F.; Li, X.; Crepin, T.; Ruigrok, R. W. Monomeric nucleoprotein of influenza A virus. *PLoS Pathog* **2013,** *9*, e1003275.

15. Kakisaka, M.; Sasaki, Y.; Yamada, K.; Kondoh, Y.; Hikono, H.; Osada, H.; Tomii, K.; Saito, T.; Aida, Y. A novel antiviral target structure involved in the RNA binding, dimerization, and nuclear export functions of the influenza A virus nucleoprotein. *PLoS Pathog* **2015,** *11*, e1005062.

16. Arranz, R.; Coloma, R.; Chichon, F. J.; Conesa, J. J.; Carrascosa, J. L.; Valpuesta, J. M.; Ortin, J.; Martin-Benito, J. The structure of native influenza virion ribonucleoproteins. *Science* **2012,** *338*, 1634-1637.

17. Pflug, A.; Guilligay, D.; Reich, S.; Cusack, S. Structure of influenza A polymerase bound to the viral RNA promoter. *Nature* **2014,** *516*, 355-360.

18. Reguera, J.; Gerlach, P.; Cusack, S. Towards a structural understanding of RNA synthesis by negative strand RNA viral polymerases. *Curr Opin Struct Biol* **2016,** *36*, 75-84.

19. Hengrung, N.; El Omari, K.; Serna Martin, I.; Vreede, F. T.; Cusack, S.; Rambo, R. P.; Vonrhein, C.; Bricogne, G.; Stuart, D. I.; Grimes, J. M.; Fodor, E. Crystal structure of the RNA-dependent RNA polymerase from influenza C virus. *Nature* **2015,** *527*, 114-117.

20. Tarus, B.; Bakowiez, O.; Chenavas, S.; Duchemin, L.; Estrozi, L. F.; Bourdieu, C.; Lejal, N.; Bernard, J.; Moudjou, M.; Chevalier, C.; Delmas, B.; Ruigrok, R. W.; Di Primo, C.; Slama-Schwok, A. Oligomerization paths of the nucleoprotein of influenza A virus. *Biochimie* **2012,** *94*, 776-785.

21. Majetich, G. Y., J. . Synthesis of Synthesis of (±)-14-epi-hydroxydolasta-1(15),7,9-triene and (±)-7-epi-acetoxy-14-epi-hydroxydolasta-1(15),8-diene. . *Can J Chem* **2012,** *90*, 75-84.

22. Rodriguez, G.; Albrecht, M.; Schoenmaker, J.; Ford, A.; Lutz, M.; Spek, A. L.; van Koten, G. Bifunctional pincer-type organometallics as substrates for organic transformations and as novel building blocks for polymetallic materials. *J Am Chem Soc* **2002,** *124*, 5127-5138.

23. Harvey, R. G.; Dai, Q.; Ran, C.; Penning, T. M. Synthesis of the o-quinones and other oxidized metabolites of polycyclic aromatic hydrocarbons implicated in carcinogenesis. *J Org Chem* **2004,** *69*, 2024-2032.

24. Di Antonio, M.; Doria, F.; Mella, M.; Merli, D.; Profumo, A.; Freccero, M. Novel naphthalene diimides as activatable precursors of bisalkylating agents, by reduction and base catalysis. *J Org Chem* **2007,** *72*, 8354-8360.

25. Maiti, D.; Buchwald, S. L. Orthogonal Cu- and Pd-based catalyst systems for the O- and N-arylation of aminophenols. *J Am Chem Soc* **2009,** *131*, 17423-17429.

26. Shuto, A.; Kushida, T.; Fukushima, T.; Kaji, H.; Yamaguchi, S. pi-Extended planarized triphenylboranes with thiophene spacers. *Org Lett* **2013,** *15*, 6234-6237.

27. Biswas, S. K.; Boutz, P. L.; Nayak, D. P. Influenza virus nucleoprotein interacts with influenza virus polymerase proteins. *J Virol* **1998,** *72*, 5493-5501.

28. Marklund, J. K.; Ye, Q.; Dong, J.; Tao, Y. J.; Krug, R. M. Sequence in the influenza A virus nucleoprotein required for viral polymerase binding and RNA synthesis. *J Virol* **2012,** *86*, 7292-7297.

29. Ng, A. K.; Chan, W. H.; Choi, S. T.; Lam, M. K.; Lau, K. F.; Chan, P. K.; Au, S. W.; Fodor, E.; Shaw, P. C. Influenza polymerase activity correlates with the strength of interaction between nucleoprotein and PB2 through the host-specific residue K/E627. *PLoS One* **2012,** *7*, e36415.

30. Vidic, J.; Noiray, M.; Bagchi, A.; Slama-Schwok, A. Identification of a novel complex between the nucleoprotein and PA(1-27) of influenza A virus polymerase. *Biochemistry* **2016,** *55*, 4259-4262.

31. Tacconelli, S.; Bruno, A.; Grande, R.; Ballerini, P.; Patrignani, P. Nonsteroidal anti-inflammatory drugs and cardiovascular safety - translating pharmacological data into clinical readouts. *Expert Opin Drug Saf* **2017**, 1-17.

32. Dudek, S. E.; Nitzsche, K.; Ludwig, S.; Ehrhardt, C. Influenza A viruses suppress cyclooxygenase-2 expression by affecting its mRNA stability. *Sci Rep* **2016,** *6*, 27275.

33. Chenavas, S.; Crepin, T.; Delmas, B.; Ruigrok, R. W.; Slama-Schwok, A. Influenza virus nucleoprotein: structure, RNA binding, oligomerization and antiviral drug target. *Future Microbiol* **2013,** *8*, 1537-1545.

34. Li, Z.; Watanabe, T.; Hatta, M.; Watanabe, S.; Nanbo, A.; Ozawa, M.; Kakugawa, S.; Shimojima, M.; Yamada, S.; Neumann, G.; Kawaoka, Y. Mutational analysis of conserved amino acids in the influenza A virus nucleoprotein. *J Virol* **2009,** *83*, 4153-4162.

35. Mondal, A.; Potts, G. K.; Dawson, A. R.; Coon, J. J.; Mehle, A. Phosphorylation at the homotypic interface regulates nucleoprotein oligomerization and assembly of the influenza virus replication machinery. *PLoS Pathog* **2015,** *11*, e1004826.

36. Daina, A.; Michielin, O.; Zoete, V. SwissADME: a free web tool to evaluate pharmacokinetics, drug-likeness and medicinal chemistry friendliness of small molecules. *Sci Rep* **2017,** *7*, 42717.

37. Lipinski, C. A.; Lombardo, F.; Dominy, B. W.; Feeney, P. J. Experimental and computational approaches to estimate solubility and permeability in drug discovery and development settings. *Adv Drug Deliv Rev* **2001,** *46*, 3-26.

38. Martin, Y. C. A bioavailability score. *J Med Chem* **2005,** *48*, 3164-3170.

39. Daina, A.; Zoete, V. A boiled-egg to predict gastrointestinal absorption and brain penetration of small molecules. *ChemMedChem* **2016,** *11*, 1117-1121.

40. Montanari, F.; Ecker, G. F. Prediction of drug-ABC-transporter interaction--recent advances and future challenges. *Adv Drug Deliv Rev* **2015,** *86*, 17-26.

41. Hung, I. F. N.; To, K. K. W.; Chan, J. F. W.; Cheng, V. C. C.; Liu, K. S. H.; Tam, A.; Chan, T. C.; Zhang, A. J.; Li, P.; Wong, T. L.; Zhang, R.; Cheung, M. K. S.; Leung, W.; Lau, J. Y. N.; Fok, M.; Chen, H.; Chan, K. H.; Yuen, K. Y. Efficacy of clarithromycin-naproxen-oseltamivir combination in the treatment of patients pospitalized for influenza A(H3N2) infection: an open-label randomized, controlled, phase IIb/III trial. *Chest* **2017,** *151*, 1069-1080.

42. Tcherniuk, S.; Cenac, N.; Comte, M.; Frouard, J.; Errazuriz-Cerda, E.; Galabov, A.; Morange, P. E.; Vergnolle, N.; Si-Tahar, M.; Alessi, M. C.; Riteau, B. Formyl peptide receptor 2 plays a deleterious role during influenza A virus infections. *J Infect Dis* **2016,** *214*, 237-247.

43. Courtin, N.; Fotso, A. F.; Fautrad, P.; Mas, F.; Alessi, M. C.; Riteau, B. Antiviral activity of formyl peptide receptor 2 antagonists against influenza viruses. *Antiviral Res* **2017,** *143*, 252-261.

44. Lejal, N.; Truchet, S.; Bechor, E.; Bouguyon, E.; Khedkar, V.; Bertho, N.; Vidic, J.; Adenot, P.; Solier, S.; Pick, E.; Slama-Schwok, A. Turning off NADPH oxidase-2 by impeding p67(phox) activation in infected mouse macrophages reduced viral entry and inflammation. *Biochim Biophys Acta* **2018,** *1862*, 1263-1275.

45. Vlahos, R.; Selemidis, S. NADPH oxidases as novel pharmacologic targets against influenza A virus infection. *Mol Pharmacol* **2014,** *86*, 747-759.

46. Phillips, J. C.; Braun, R.; Wang, W.; Gumbart, J.; Tajkhorshid, E.; Villa, E.; Chipot, C.; Skeel, R. D.; Kale, L.; Schulten, K. Scalable molecular dynamics with NAMD. *J Comput Chem* **2005,** *26*, 1781-1802.

47. MacKerell, A. D., Jr.; Banavali, N.; Foloppe, N. Development and current status of the CHARMM force field for nucleic acids. *Biopolymers* **2000,** *56*, 257-265.

48. Jorgensen, W. L.; Chandrasekhar, J.; Madura, J. D.; Impey, R. W.; Klein, M. L. Comparison of simple potential functions for simulating liquid water. *J. Chem. Physiol.* **1983,** *79*, 926-935.

49. Darden, T.; York, D. M.; Pedersen, L. Particle mesh Ewald: An N×log(N) method for Ewald sums in large systems. . *J. Chem. Phys.* **1993,** *98*, 10089-10092.

50. Venkatachalam, C. M.; Jiang, X.; Oldfield, T.; Waldman, M. LigandFit: a novel method for the shape-directed rapid docking of ligands to protein active sites. *J Mol Graph Model* **2003,** *21*, 289-307.

51. Slama Schwok, A.; Delmas, B.; Quideau, Q.; Bertrand, H.; Tarus, T.; Antiviral compositions directed against the nucleoprotein of influenza viruses US Patent US20180028478A1, February 1, 2018.

Legends to Figures :

Figure 1: Comparison of the binding of the naproxen analogues to NP after 40 ns MD simulations. A-E: Chemical structures and binding modes of Naproxen and its derivatives. N, O and H atoms are colored blue, red and grey, respectively. The surface of the enzyme is colored according the capacity of the residues to donate (purple) or accept (green) hydrogen bonds. See also Table 1 that describes the molecular interactions involved in the derivatives binding to NP

F: Overview of the binding sites of Naproxen (black) and derivative **1**[5] (yellow), **2**[6] (cyan), **3** (orange), and **4** (green). The surface of the enzyme is colored according its polar and non-polar regions (from blue to brown, respectively). Note the different binding site of derivative **4** as compared to that observed for naproxen, derivatives **1**-**3**. The naproxen moiety of derivative **4** remained buried as for derivative **2**, its aminophenol part being well recognized while the naphthalene moiety of derivative **3** tends to be less buried that its aminophenol moiety.

Figure 2: A-B: Induced fit of NP wt structure as a result of binding of derivative **4** (noted D4 and shown in green) and comparison with ligand-free NP wt (red) or its mutant R416A (blue). Note the large change in the oligomerization loop, loops 1 and 2 of NP. C-D: changes in the cavity around E339 receiving the oligomerization loop from next monomer in NP trimer[8], with a clear decrease in the volume of the cavity induced by the presence of derivative **4** (green) as compared to ligand-free NP (red). The volume of the cavity in the mutant R416A (blue) is also indicated for comparison.

Figure 3 : Evidence of a PA(1-27)-NP complex formed with NP disrupted by some of the naproxen analogues: **A**: Commassie blue and western blots showing that recombinant NP or NP from infected cell lysate forms a complex with PA(1-27) that is disrupted by addition of

derivatives **2**, **3** and **4** but not by naproxen or derivative **1**. **B**: a,b: SPR evaluation of the NP-PA(1-27) or NP-PA(1-27)-DNA complexes and its specific disruption by derivative **2**; c: in contrast, naproxen is unable to compete with NP-PA(1-27)-DNA complex, even at a concentration of 50 μM; d: dose-response competition of derivative **2** with the NP-PA(1-27)-DNA complex.

Figure 4: Evaluation of the putative therapeutic window of A: naproxen, B: derivative **2** and C: derivative **4** in MDCK cells challenged with Influenza A/WSN/33 (H3N2) at MOI = 2 after 18 hours (see also Table 3). The toxicity is evaluated by the MTT assay while the NP levels are determined by immunofluorescence (corrected for cell viability loss by assessing DAPI levels). It is represented as a ratio of treated versus untreated infected cells.

Figure 5: Evaluation of the antiviral properties of derivatives **2**, **3** and **4** against the pandemic *A/Netherlands*/602/09 Influenza virus in MDCK cells (see also Table 5) by immunofluorescence using a red-labeled NP monoclonal antibody.

Figure 6: A-B: Evaluation of the antiviral properties of derivatives **2**, **3** and **4** the towards MDCK cells against Oseltamivir-resistant PR8 virus (corrected for cell viability loss by assessing DAPI levels). C-D: Evaluation of Oseltamivir treatment in MDCK cells infected with C: Oseltamivir-resistant or D: PR8 oseltamivir-sensitive virus - (see also Table 6). The NP levels were determined by immunofluorescence using a red-labeled NP monoclonal antibody.

Figure 7: A549 cells pre-treated with naproxen or derivative **4** or untreated during 30 minutes were infected with IAV at MOI 2 during 18 hours or activated with γ-ATP in the presence or absence of derivatives **2** and **3**. The levels of COX2 produced in the cell supernatants were quantified by IF using a monoclonal antibody as detailed in the experimental section.

Figure 8: *In vivo* evaluation of the antiviral effect of derivative **2** compared to that of naproxen in a mouse model of intranasal IAV challenge with 500 pfu/mouse. The mice were treated immediately after infection at day 0 and at day 1 and 2 (a total of three IP injections) with the indicated amount of drugs or vehicle. **A**- Survival curves. The p value compared to untreated control was p = 0.0003 for treatment with 8 mg of derivative 2 or oseltamivir; the statistical difference between 1 mg of derivative **2** compared to 1 mg naproxen was p= 0.024. The dose 1 mg/mouse corresponds to 50 mg/kg. **B**- Body weight curves; the statistical difference between 8 mg of derivative **2** compared to untreated control was p= 0.0004. The dose 8 mg/mouse corresponds to 400 mg/kg **C**- Viral titers of the mice sacrificed at day 2 post-infection. The statistical differences compared to untreated control are 0.0159 for naproxen and derivative **2** 1 mg, 0.0022 and 0.0079 for 8 mg derivative 2 and oseltamivir.

Legends to Schemes :

Scheme 1: Chemical synthesis of derivative 4 (12): *Reagents and conditions*: i) Br_2 (1.1 equiv.), cat. Fe, anhydrous CH_2Cl_2, 39 °C, 2 h (93%); ii) Fe (1.0 equiv.), AcOH, 80 °C, overnight (90%); iii) HCl 37%, aq. $NaNO_2$ (3.0 equiv., 2.35 M), 0 °C, 1 h, then aq. KI (5.0 equiv., 2.61 M), 0 °C, 30 min, then reflux, 1 h (60%); iv) $KMnO_4$ (6.0 equiv.), *t*-BuOH/H_2O (1:2), reflux, overnight (65%); v) MeOH, conc. H_2SO_4, reflux, 16 h (83%); vi) MeI (3.0 equiv.), K_2CO_3 (3.0 equiv.), acetone, overnight (77%); vii) **7** (1.1 equiv.), $Pd(PPh_3)_4$ (0.05 equiv.), aq. K_2CO_3 (2.0 equiv.), 1,4-dioxane, reflux, 4 h (47%); viii) **9** (1.5 equiv.), CuI (0.10 equiv.), picolinic acid (0.20 equiv.) K_3PO_4 (2.0 equiv.), dry DMF, reflux (110 °C), 24 h (10%); ix) 1 N HCl, 1,4-dioxane, 95 °C, 3 h (100%); x) aq. KOH (20.0 equiv.), THF, reflux, 13 h (50%).

Scheme 2: Chemical synthesis of derivative 3 (20) : *Reagents and conditions*: i) HCl 37%, aq. $NaNO_2$ (3.0 equiv.), 0 °C, 1 h, then aq. KI (5.0 equiv.), 0 °C, 30 min, then reflux, 1 h (100%); ii) $KMnO_4$ (6.0 equiv.), *t*-BuOH/H_2O (1:2), reflux, overnight (60%); iii) MeOH, conc. H_2SO_4, reflux, 16 h (80%); iv) **7** (1.1 equiv.), $Pd(PPh_3)_4$ (0.05 equiv.), aq. K_2CO_3 (2.0 equiv.), 1,4-dioxane, reflux, 6 h (40%); v) **9** (1.5 equiv.), CuI (0.10 equiv.), picolinic acid (0.20 equiv.) K_3PO_4 (2.0 equiv.), dry DMF, reflux (110 °C), 24 h (10%); vi) 1 N HCl, 1,4-dioxane, 95 °C, 3 h (100%); vii) aq. KOH (20.0 equiv.), THF, reflux, 13 h (50%).

Table 1 : Free Binding Energy Estimation and molecular interactions of Naproxen and its derivatives (HB= hydrogen bond ; VDW= Van Der Waals interactions)

Ligands	Free Binding Energy (Kcal/mol)	Molecular interactions
Naproxen	-24	-Naphtalene : π -cation and π -alkyl with R355 -COO^- : salt bridge and HB with R361
Derivative **1**	-80[a]	-Naphtalene : π– alkyl, π -amide with R355 and VDW with G356 -COO^- 1 : salt bridge and HB with R152 -COO^- 2 : salt bridge and HB with R355
Derivative **2**	-52	Naphtalene : π -stacking with Y148 and π-cation with R361 -COO^- 1 : salt bridge and HB with R361 -COO^- 2 : HB with N149 -phenyl: π -alkyl with R152 and π -donor with N149
Derivative **3**	-68	-COO^- 1 : 2 HB with N149 -COO^- 2 : salt bridge and HB with R361 and R355 - phenyl: π -cation with R355 -aminophenol : π -donor with Y148 and π -cation with R361
Derivative **4**	-86	Naphtalene : π -cation with R152 and R156 -COO^- 1 : HB and salt bridge

		with R152 -COO^- 2 : HB and salt bridge with R195 -phenyl: amide- π stacked with R152 and π -alkyl with A153 - aminophenol : π - π T-shaped with Y148 and cation –π with R150

a: this energy corresponds to the most stable complex while there is another population with a lower energy close to that of derivative 2.

Table 2: Comparison of the naproxen derivatives: binding affinities and antiviral effect in protecting MDCK cells against Influenza A/WSN/33

Compound	**Ki NP (nM) / Tm °C**	**Ki PA(1-27) [c, d] (µM)**	**IC_{50} (µM) MOI 10^{-3}**	**IC_{50} (µM) MOI 2**	**CC_{50} [e, f] (mM)**	**SI= CC_{50}/IC_{50} MOI 10^{-3}**	**SI MOI 2**
Naproxen	250±50 [a] / 41±1°	none [c,d]	16± 5	100 ± 15	1.4 ± 0.5 [e] (ref 5) 1.0 ± 0.3 [f]	87	14
Derivative 1	800 ± 100 [b] / biphasic ~ 25 and 45±1°[b]	none [c]					
Derivative 2	97± 25/ 46±1°	Displaced [c] 30 ± 10[d]	2.9 ± 0.4	19 ± 4	13 ± 2 [e] 10 ± 3 [f]	4483	684
Derivative 3	38°, 47±1° biphasic	Displaced [c]			13 ± 2 [e] ≥ 10 [f]		
Derivative 4	30 ± 10/ 48±1°	Displaced [c]	1.3 ± 0.2	13 ± 4	12 ± 2 [e] ≥ 10 [f]	9230	923

a: [5]; b: [6] in agreement with the MD simulations, the biphasic melting curve of NP with derivative **1** that showed Tm = 25 and 45°C likely reflected at least two binding sites of this derivative to NP; accordingly, the SPR data show an inhibition of only ~30% the NP-RNA complex is displaced by derivative **1** in the concentration range 0.01-1 µM while at concentration from 1 to 10µM, this inhibition decreased to zero (See Figure 4 in reference 6); c: from WB analysis (Figure 3A) none: no displacement of the NP-PA(1-27) complex, displaced: the derivative competes with the NP-PA(1-27) complex. d: from SPR measurements (Figure 3B). e: determined by MTT tests at 48H; f: determined by cell counting with trypan blue staining at 48h; nd: not determined

Table 3: Comparison of antiviral protection of A549 cells by naproxen, derivatives 2 and 4 18 hours after a viral challenge at MOI = 2 with Influenza A/Udorn/72 (H3N2) virus.

Compound	**IC_{50} (µM)**	**CC_{50} (mM)**	**SI**
Naproxen[a]	112 ± 21	1.4 ± 0.5	12.5
Derivative 2	25 ± 5	13 ± 2	520
Derivative 4	17 ± 4	12 ± 2	706

a: [5]

Table 4: Comparison of antiviral protection of MDCK cells by naproxen, derivatives 2 and 4 18 hours after a viral challenge at the specified MOI with Influenza A/Udorn/72 (H3N2) virus

Compound	**IC_{50} (µM) MOI 10^{-3}**	**IC_{50} (µM) MOI 0.2**	**IC_{50} (µM) MOI 2**	**SI MOI 2**
Naproxen[a]			120 ± 25	12
Derivative 2	2.0 ± 0.5	7 ± 2	20 ± 5	650
Derivative 4			13 ± 4	923

a: [5]

Table 5: Comparison of antiviral protection of MDCK cells by derivatives 2, 3 and 4 18 hours after a viral challenge at MOI = 10^{-3} with Influenza A/pdm/ (H1N1 2009) virus

Compound	**IC_{50} (µM)**	**CC_{50} (mM)**	**SI**
Derivative 2	1.8 ± 0.2	13 ± 2	7222
Derivative 3	21 ± 5	13 ± 2	619
Derivative 4	0.7 ± 0.1	12 ± 2	17143

Table 6: Comparison of antiviral protection of MDCK cells by naproxen, derivatives 2 and 4 18 hours after a viral challenge at MOI = 10^{-3} with Influenza A/PR8/ (H1N1 tamiflu-resistant) virus

Compound	**IC_{50} (µM)**	**CC_{50} (mM)**	**SI**
Derivative 2	8.8 ± 2.5	13 ± 2	1477
Derivative 3	8.0 ± 0.7	13 ± 2	1625
Derivative 4	1.0 ± 0.2	12 ± 2	12000

Table 7: Prediction of some pharmacokinetics properties of Naproxen and its derivatives.

1) Evaluation of six physicochemical properties (lipophilicity, size, polarity, solubility, flexibility and saturation) for a rapid appraisal of drug-likeness [36]. A Physicochemical range on each axis is defined by descriptors adapted from Ritchie et al[51] and Lovering et al[52] and depicted as a pink area in which the radar plot of the molecule has to fall to be considered drug-like.

2) Lipinski's rules indicates the probability of a compound to be an oral drug (i.e. the drug-likeness) [37]. Abbot Bioavailability Score indicating the probability of a compound to have at least 10% oral bioavailability in rat or measurable Caco-2 permeability [38].

3) Binary classification model for passive human gastrointestinal [39].

4) SVM (Support Vector Machines)-based model for detecting the probability of a molecule to be a substrate of the P-glycoprotein (i.e. capacity to undergo efflux through biological membranes) [40].

Compounds	Bioavailability radar[1]	Lipinski's rules / Abbot bioavailability Score [2]	GI absorption[3]	P-gp substrate[4]
Naproxen	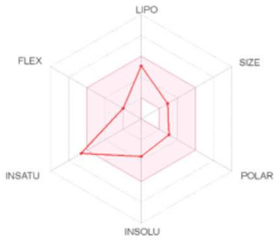	No violation /0.56	HIGH	NO
Derivative 1	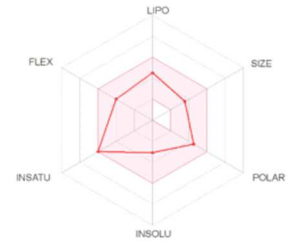	No violation /0.56	HIGH	NO
Derivative 2	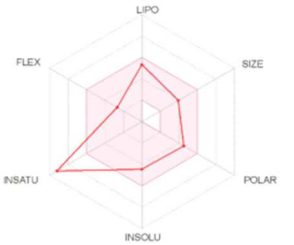	No violation /0.56	HIGH	NO
Derivative 3		No violation /0.56	HIGH	NO
Derivative 4		No violation /0.56	HIGH	NO

Figure 1

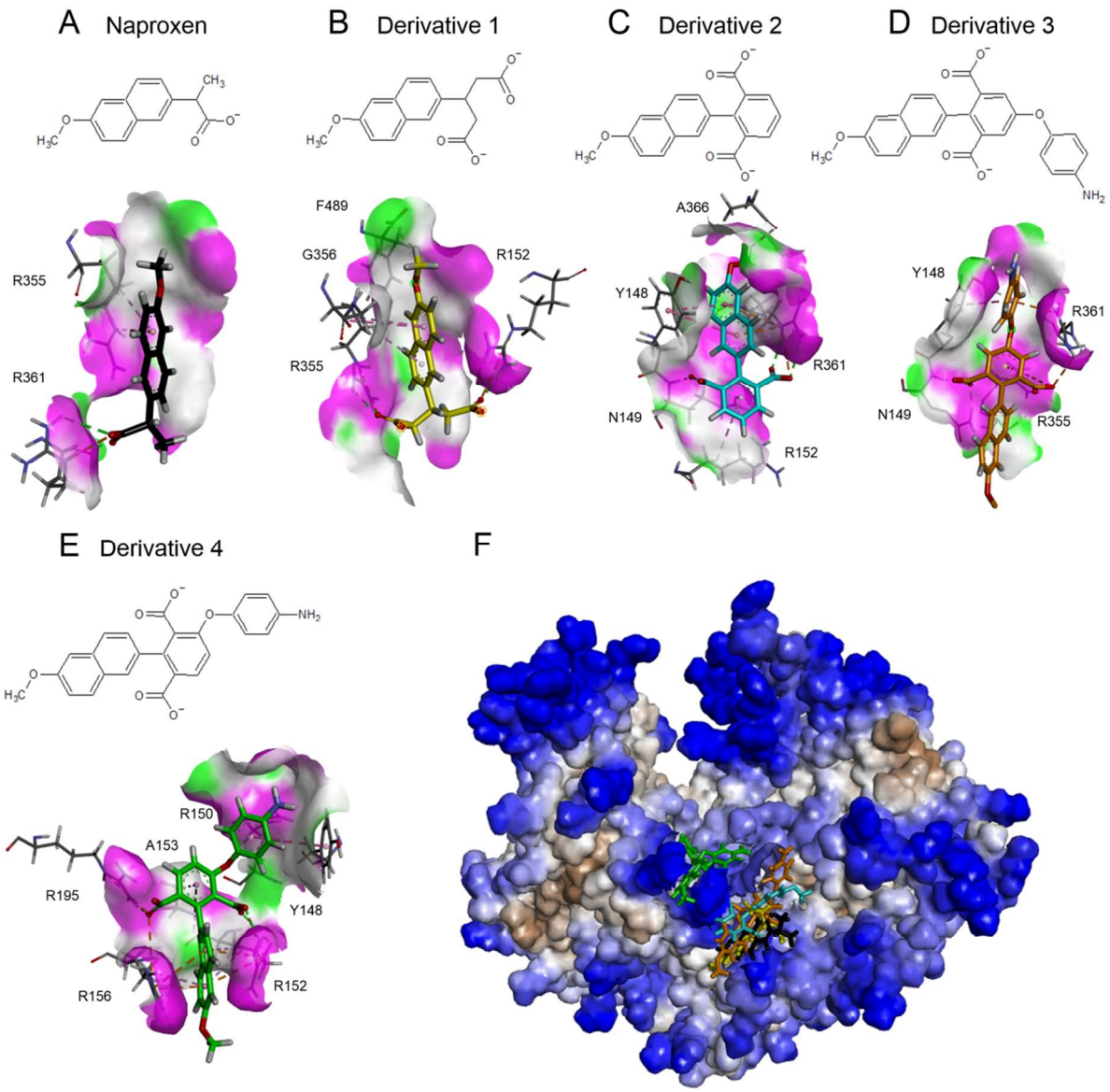
A Naproxen
B Derivative 1
C Derivative 2
D Derivative 3
E Derivative 4
F
R355
R361
F489
G356
R152
R355
A366
Y148
R361
N149
R152
Y148
R361
N149
R355
R150
A153
R195
Y148
R156
R152

Figure 2:

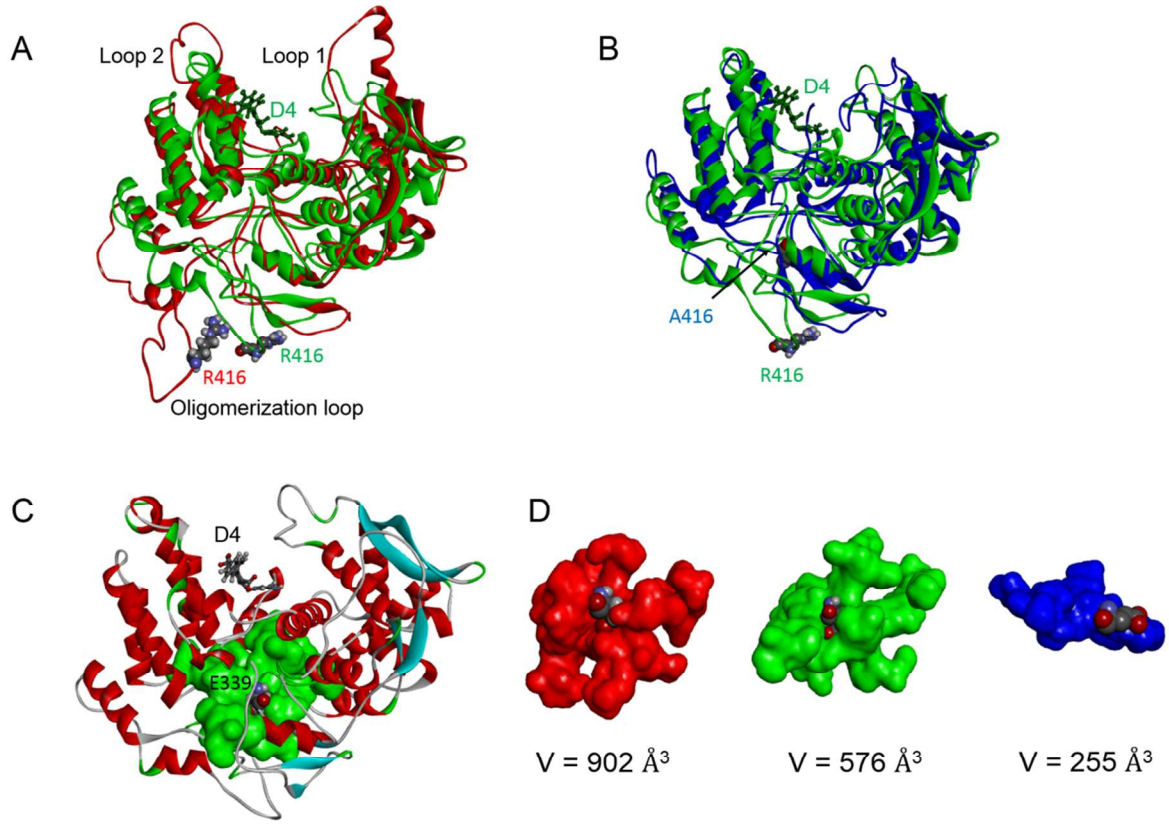
A
Loop 2
Loop 1
D4
R416
R416
Oligomerization loop
B
D4
A416
R416
C
D4
E339
D
V = 902 Å³
V = 576 Å³
V = 255 Å³

Figure 3

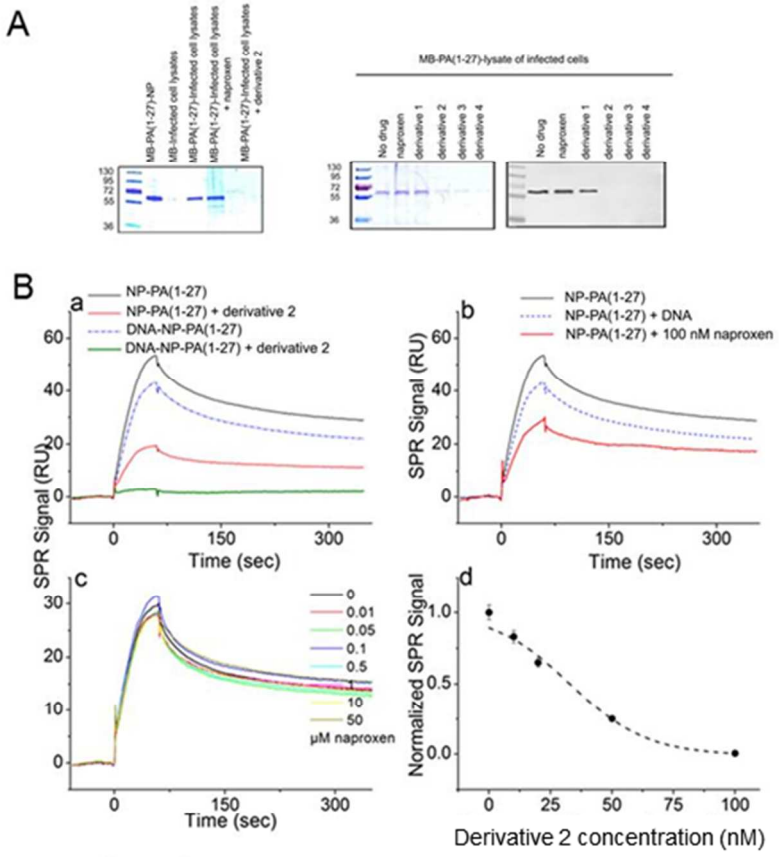
A
MB-PA(1-27)-NP
MB-infected cell lysates
MB-PA(1-27)-infected cell lysates
MB-PA(1-27)-infected cell lysates + naproxen
MB-PA(1-27)-infected cell lysates + derivative 2
MB-PA(1-27)-lysate of infected cells
No drug
naproxen
derivative 1
derivative 2
derivative 3
derivative 4
130
95
72
55
36
B
a
NP-PA(1-27)
NP-PA(1-27) + derivative 2
DNA-NP-PA(1-27)
DNA-NP-PA(1-27) + derivative 2
SPR Signal (RU)
Time (sec)
b
NP-PA(1-27)
NP-PA(1-27) + DNA
NP-PA(1-27) + 100 nM naproxen
c
0
0.01
0.05
0.1
0.5
10
50
μM naproxen
d
Normalized SPR Signal
Derivative 2 concentration (nM)

Figure 4:

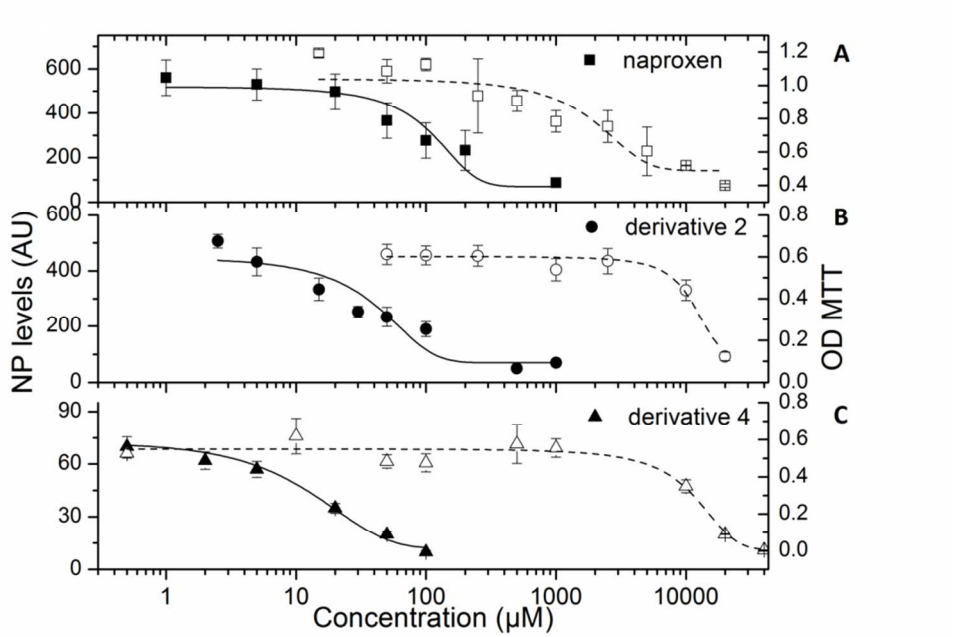
naproxen
derivative 2
derivative 4
A
B
C
NP levels (AU)
OD MTT
Concentration (μM)
1
10
100
1000
10000

Figure 5

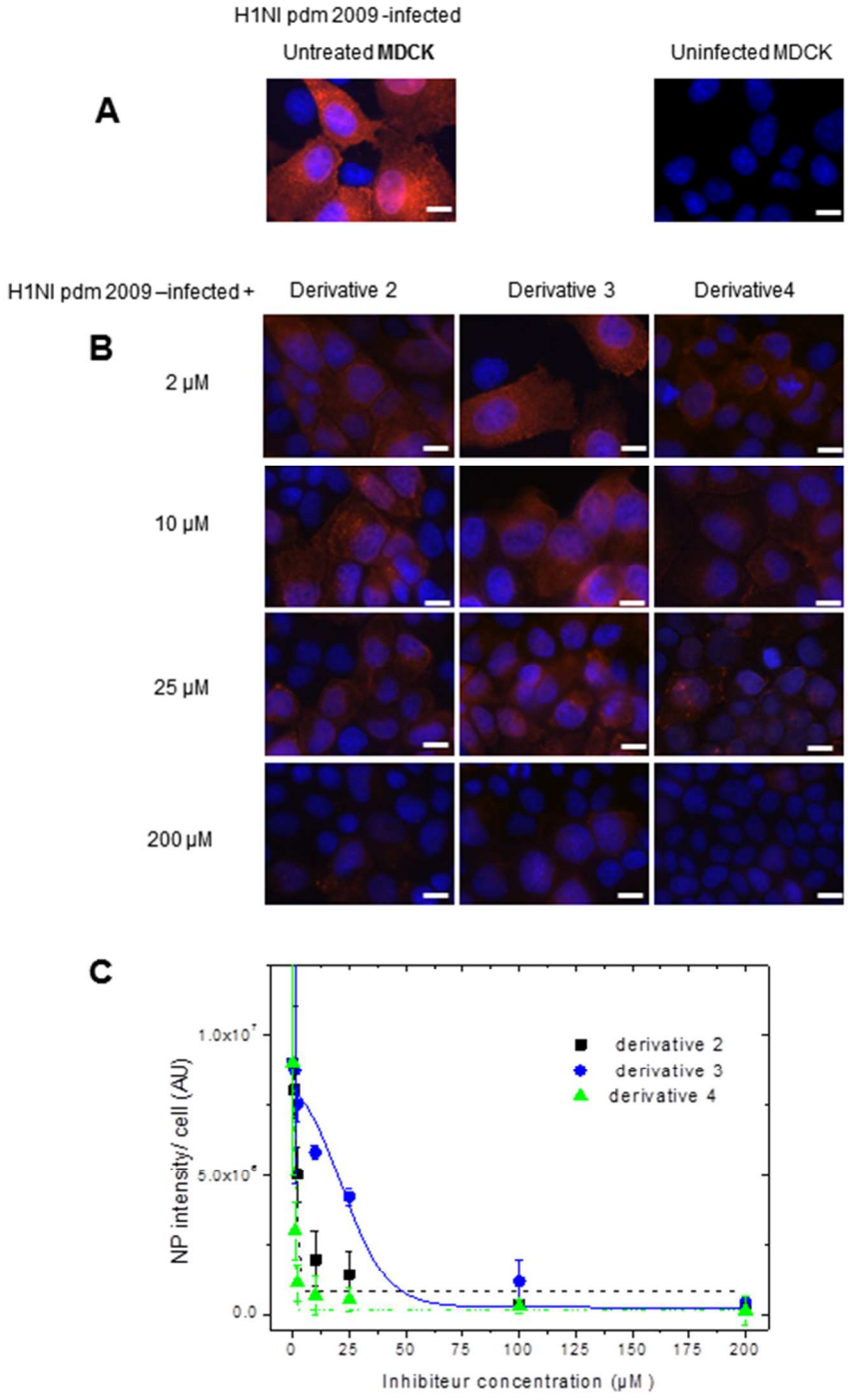
H1NI pdm 2009 -infected
Untreated MDCK
Uninfected MDCK
A
H1NI pdm 2009 –infected +
Derivative 2
Derivative 3
Derivative4
B
2 µM
10 µM
25 µM
200 µM
C
NP intensity/ cell (AU)
1.0x10^7
5.0x10^6
0.0
derivative 2
derivative 3
derivative 4
0
25
50
75
100
125
150
175
200
Inhibiteur concentration (µM)

Figure 6

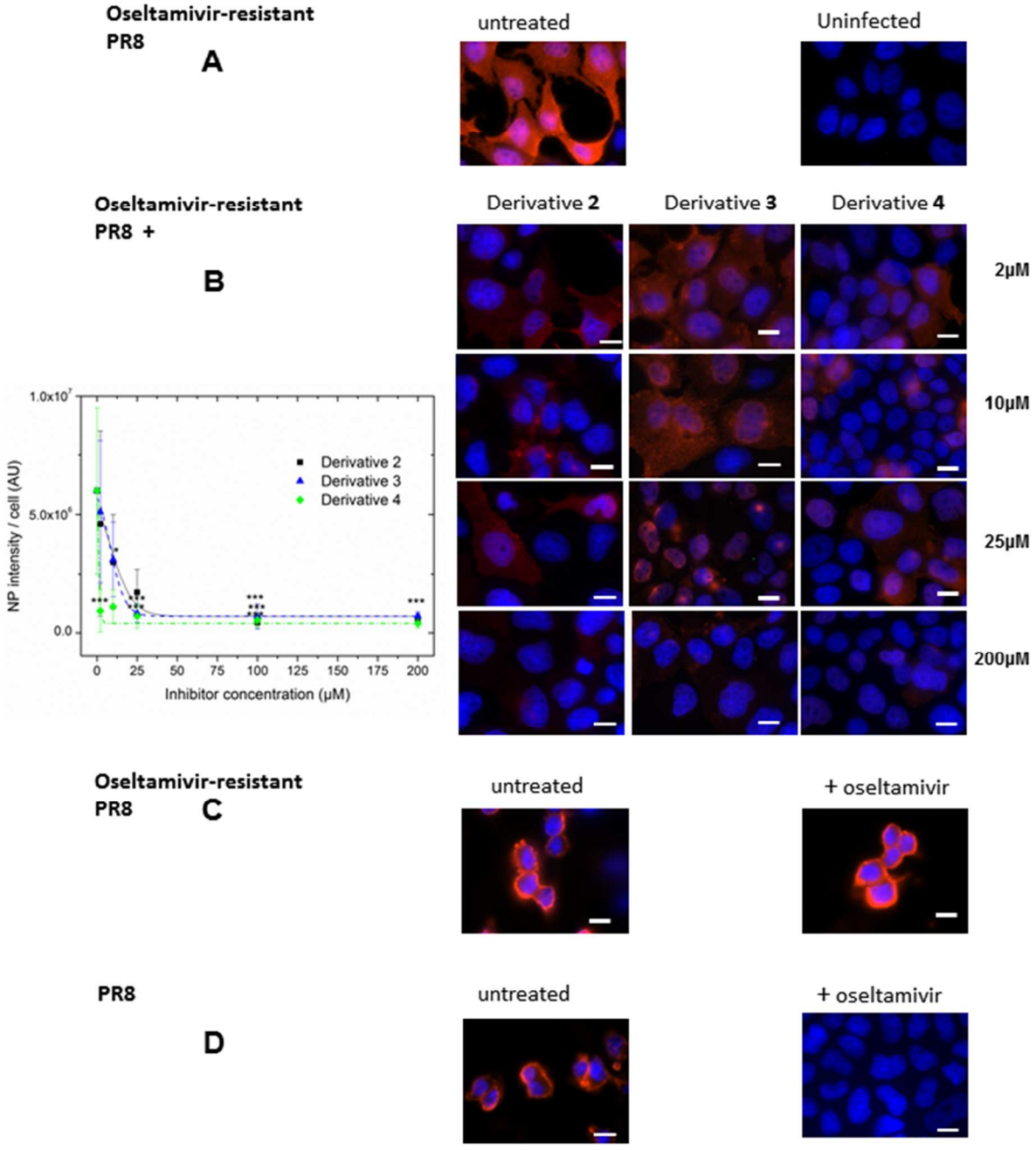
Oseltamivir-resistant
PR8
A
untreated
Uninfected
Oseltamivir-resistant
PR8 +
B
Derivative 2
Derivative 3
Derivative 4
2μM
10μM
25μM
200μM
NP intensity / cell (AU)
1.0x10^7
5.0x10^6
0.0
0
25
50
75
100
125
150
175
200
Inhibitor concentration (μM)
Derivative 2
Derivative 3
Derivative 4
Oseltamivir-resistant
PR8
C
untreated
+ oseltamivir
PR8
D
untreated
+ oseltamivir

Figure 7

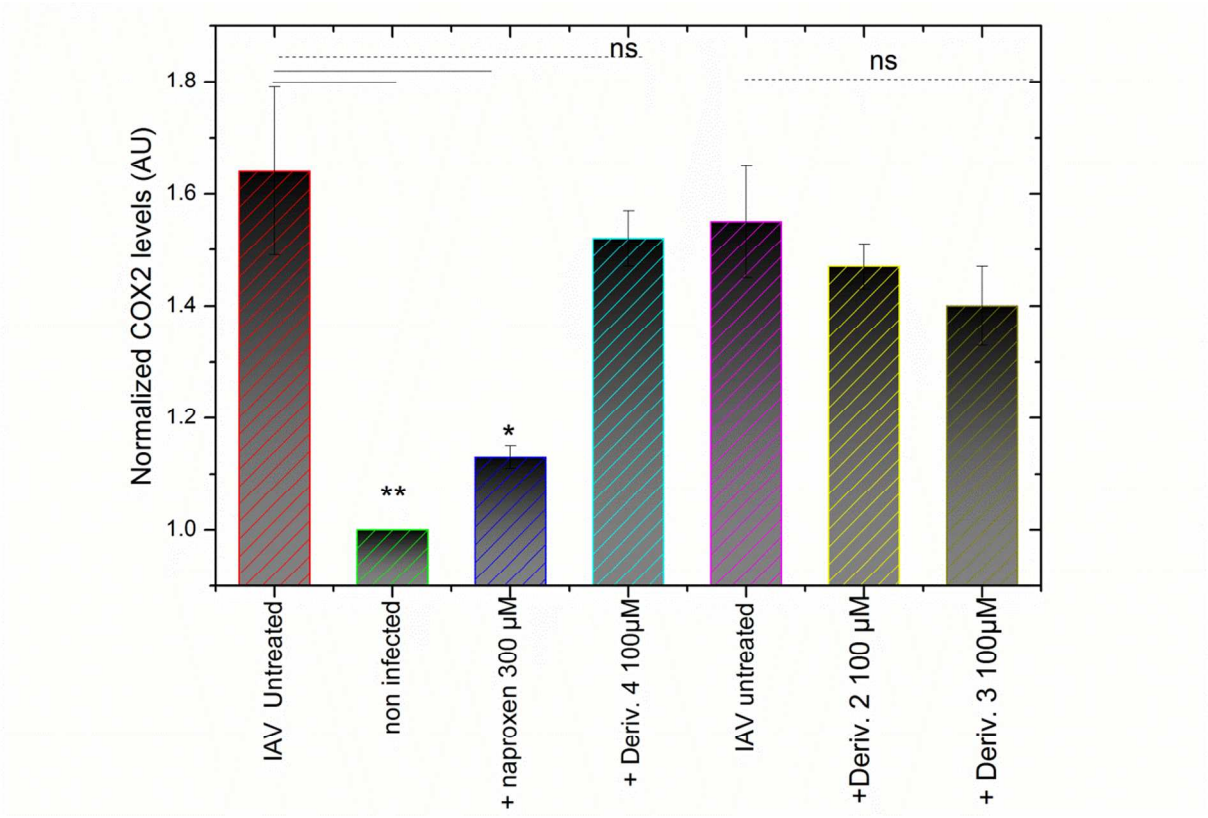
Normalized COX2 levels (AU)
1.0
1.2
1.4
1.6
1.8
ns
ns
**
*
IAV Untreated
non infected
+ naproxen 300 µM
+ Deriv. 4 100µM
IAV untreated
+Deriv. 2 100 µM
+ Deriv. 3 100µM

Figure 8

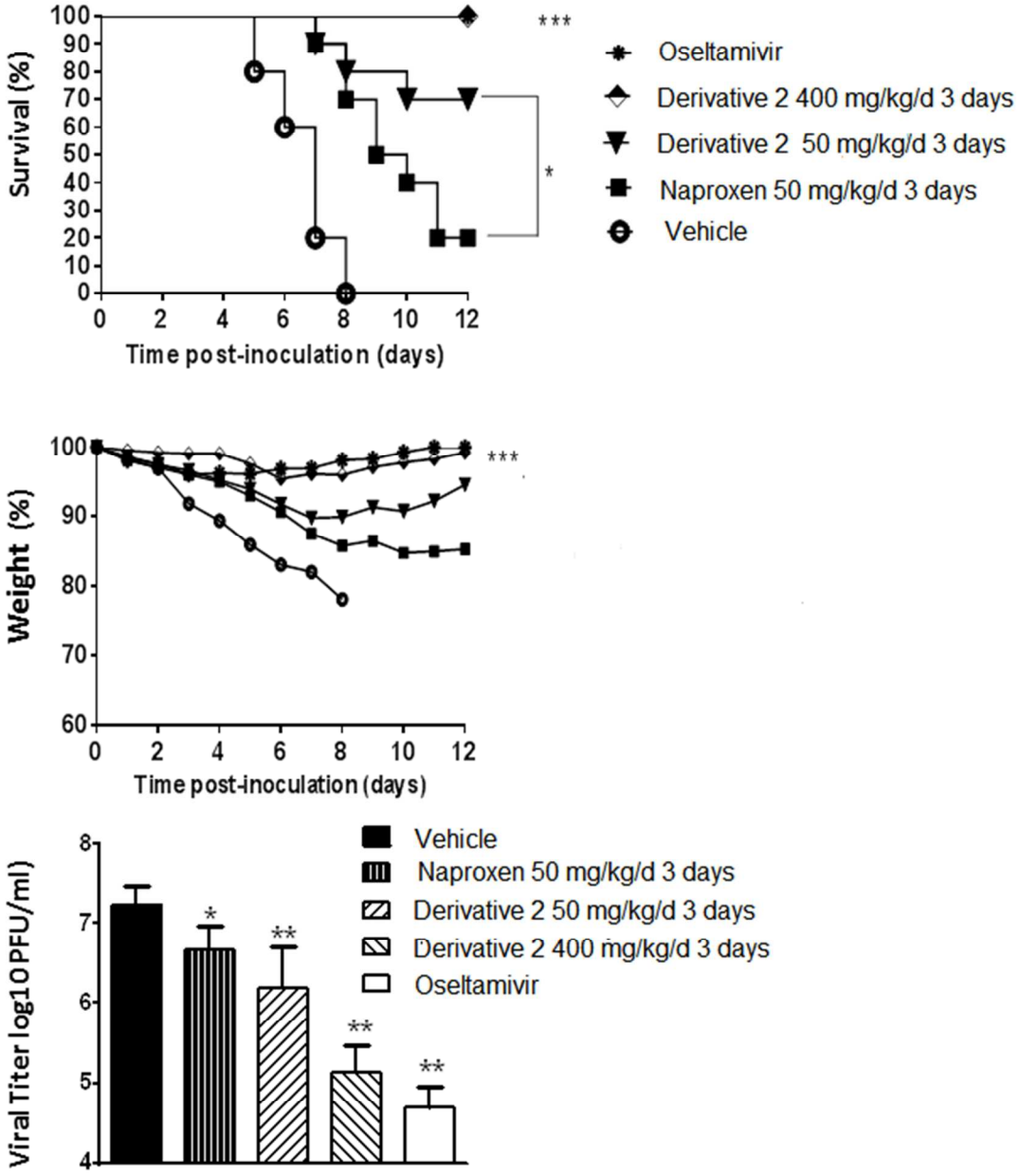
Survival (%)
Time post-inoculation (days)
***
*
Oseltamivir
Derivative 2 400 mg/kg/d 3 days
Derivative 2 50 mg/kg/d 3 days
Naproxen 50 mg/kg/d 3 days
Vehicle
Weight (%)
Time post-inoculation (days)
***
Viral Titer log10PFU/ml)
Vehicle
Naproxen 50 mg/kg/d 3 days
Derivative 2 50 mg/kg/d 3 days
Derivative 2 400 mg/kg/d 3 days
Oseltamivir
*
**
**
**

Scheme 1

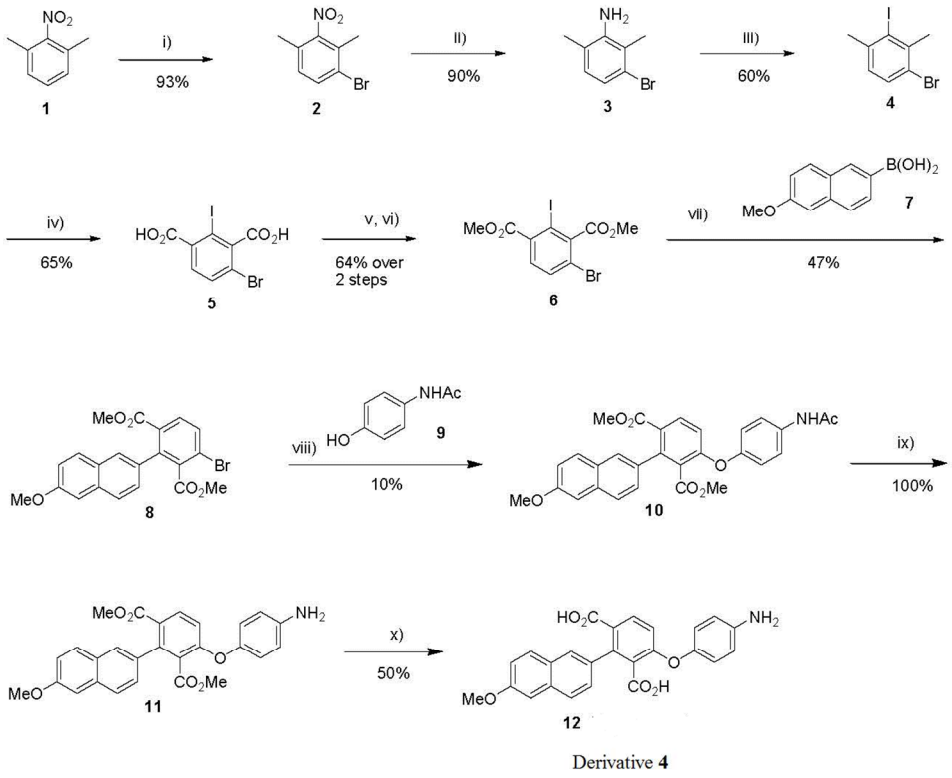

Derivative **4**

Scheme 2

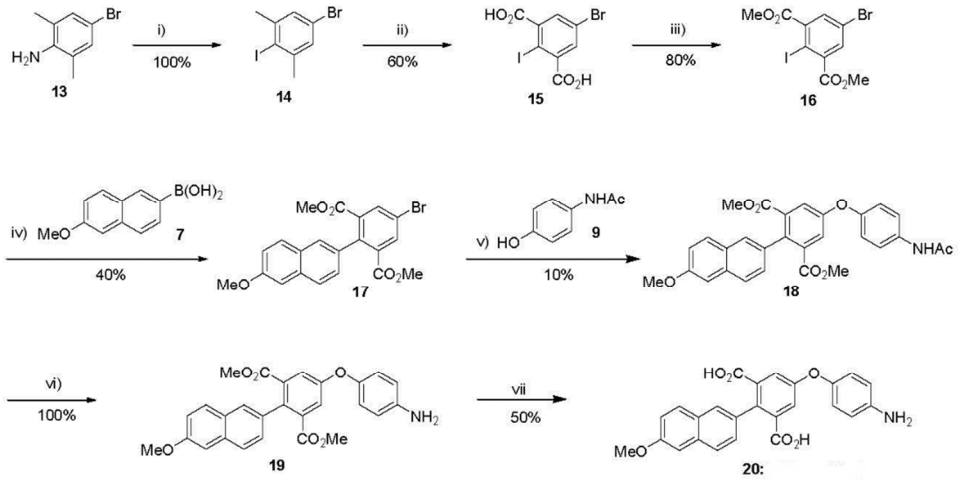

Derivative **3**

Table of Contents graphic

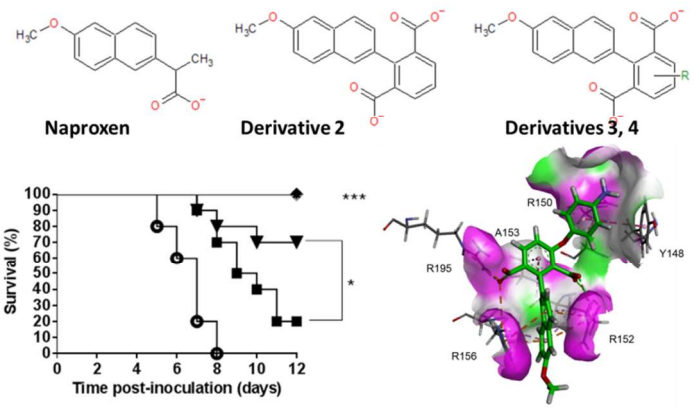

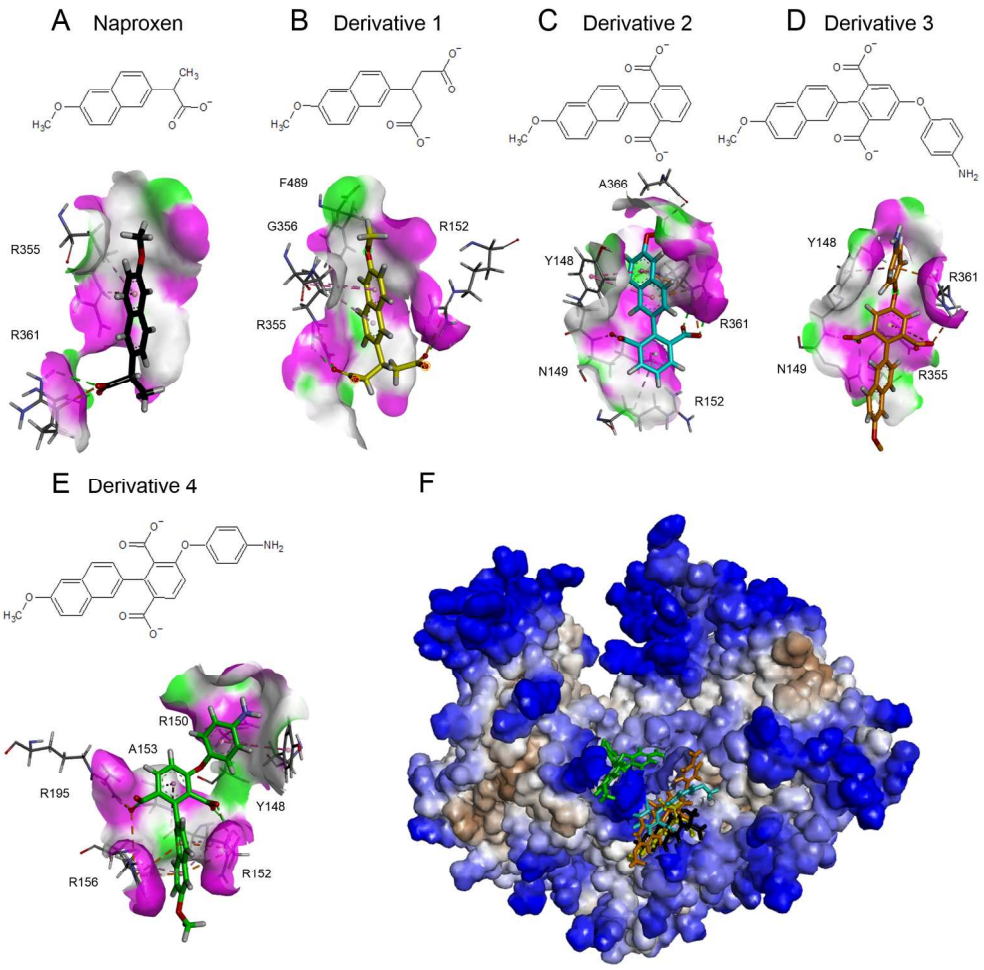

Figure 1

339x331mm (150 x 150 DPI)

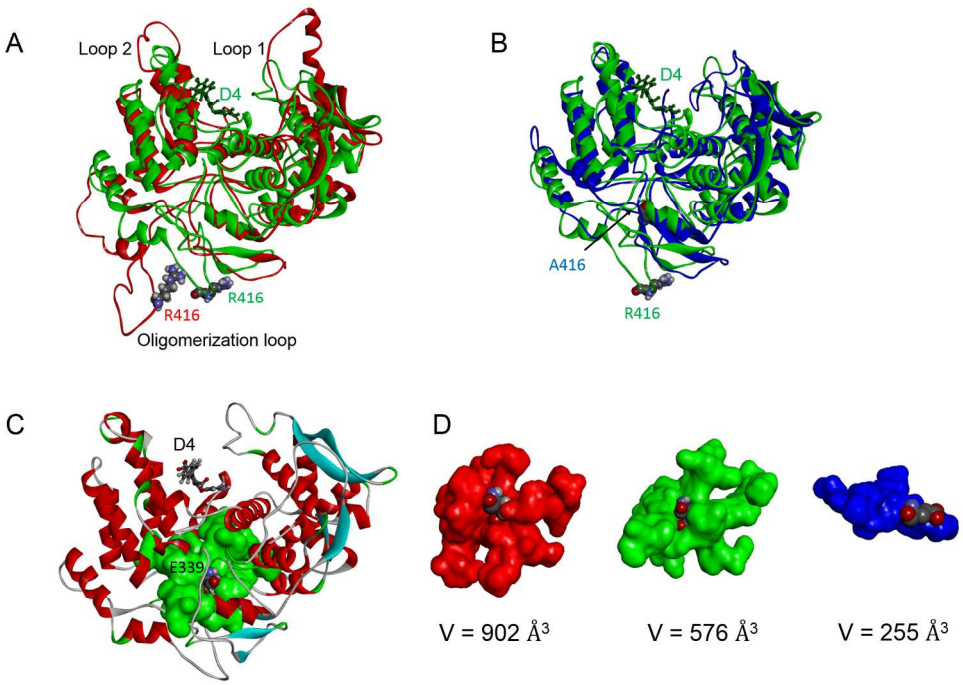

Figure 2

362x251mm (150 x 150 DPI)

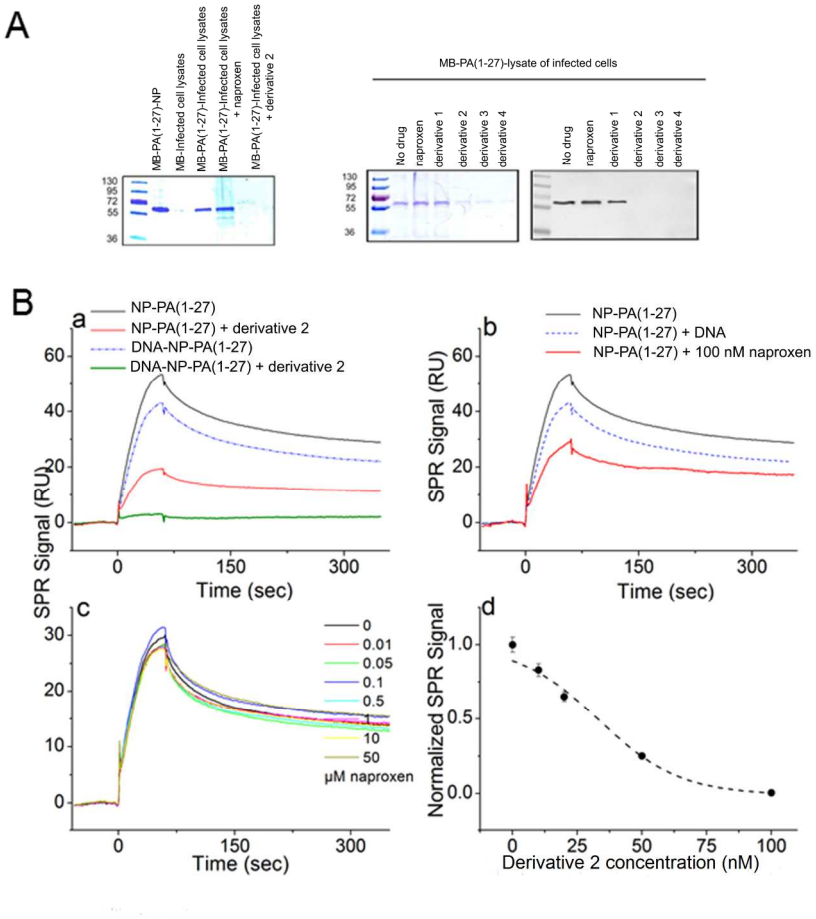

Figure 2

Figure 3

226x302mm (300 x 300 DPI)

Figure 3

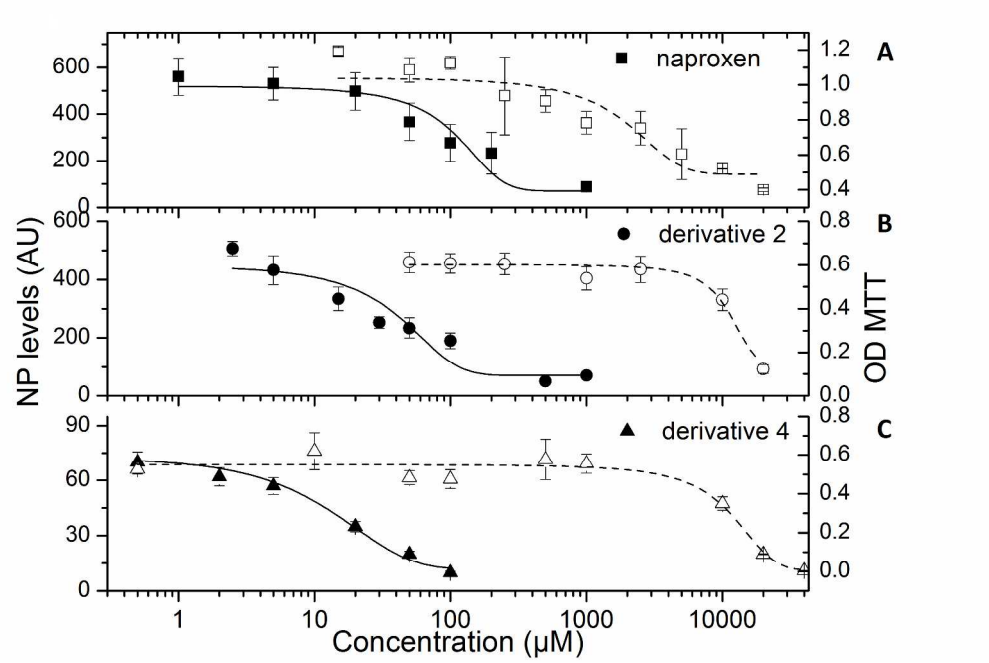

Figure 4

901x629mm (96 x 96 DPI)

Figure 4

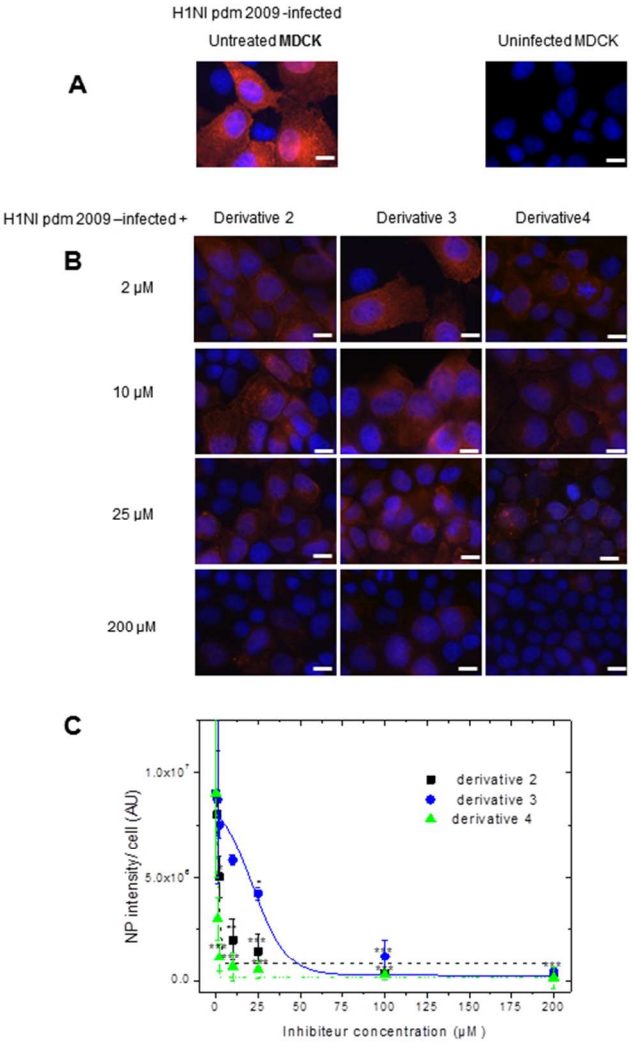

Figure 5

190x254mm (96 x 96 DPI)

Figure 5

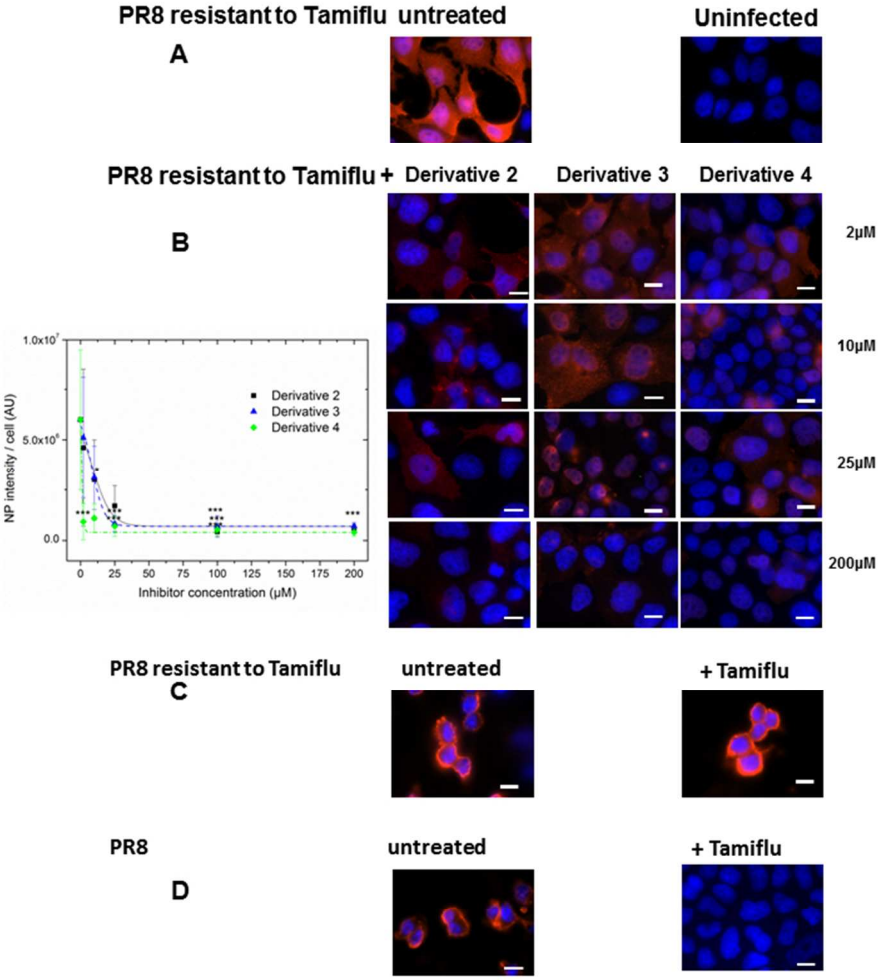

Figure 6

190x254mm (96 x 96 DPI)

Figure 6

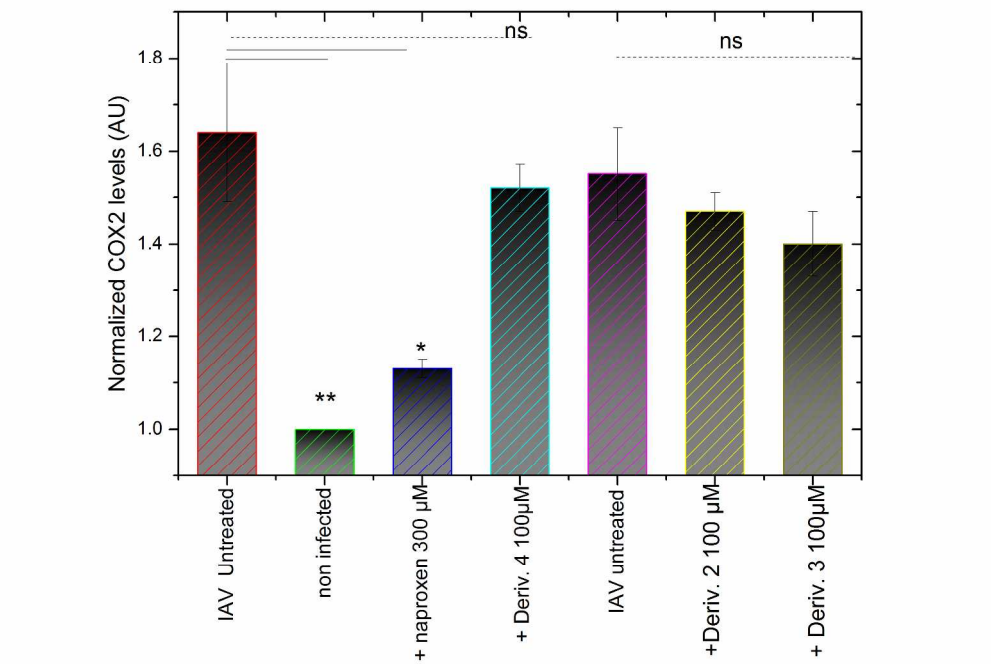

Figure 7

287x201mm (300 x 300 DPI)

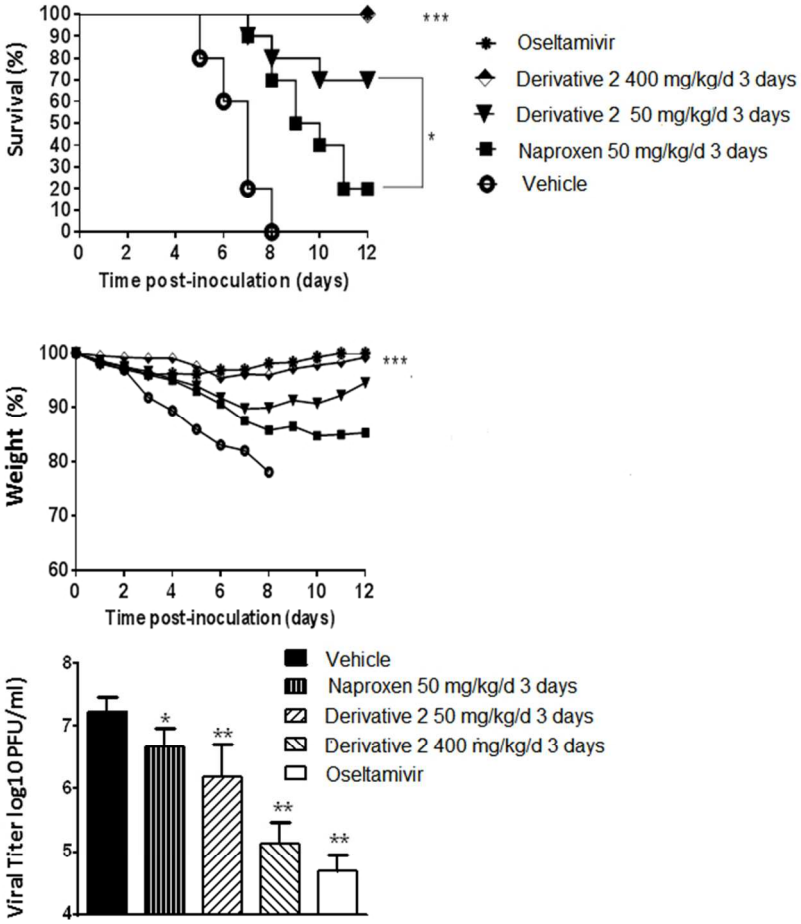

Figure 8

190x254mm (96 x 96 DPI)